PIWI-mediated control of tissue-specific transposons is essential for somatic cell differentiation

Danyan Li[1], David H. Taylor[1], Josien C. van Wolfswinkel[1,2,*]

[1]Department of Molecular Cellular and Developmental Biology, Yale University, New Haven, CT 06511, USA

[2]Lead contact

SUMMARY

PIWI proteins are known as mediators of transposon silencing in animal germlines but are also found in adult pluripotent stem cells of highly regenerative animals, where they are essential for regeneration. Study of the nuclear PIWI protein SMEDWI-2 in the planarian somatic stem cell system reveals an intricate interplay between transposons and cell differentiation in which a subset of transposons is inevitably activated during cell differentiation, and the PIWI protein is required to regain control. Absence of SMEDWI-2 leads to tissue-specific transposon derepression related to cell-type-specific chromatin remodeling events and in addition causes reduced accessibility of lineage-specific genes and defective cell differentiation, resulting in fatal tissue dysfunction. Finally, we show that additional PIWI proteins provide a stem-cell-specific second layer of protection in planarian neoblasts. These findings reveal a far-reaching role of PIWI proteins and PIWI-interacting RNAs (piRNAs) in stem cell biology and cell differentiation.

Graphical Abstract

In brief

Chromatin reorganization is an essential part of cell differentiation but risks reactivation of silenced repetitive elements. Li et al. show that planarians use continuous surveillance by a nuclear PIWI protein to chaperone the chromatin transition from pluripotent to differentiated cell, which is crucial for the planarian's impressive regeneration and homeostasis.

INTRODUCTION

PIWI-interacting RNAs (piRNAs) underlie a highly conserved regulatory mechanism with profound effects on animal fertility and protect the animal germline against the mutagenic consequences of transposon activity (Aravin et al., 2006; Girard et al., 2006; Grivna et al., 2006; Aravin et al., 2007; Brennecke et al., 2007; Carmell et al., 2007). They rely strictly on a family of small RNA-binding proteins, the PIWI proteins, for their biogenesis and their mechanism of action (Cox et al., 1998; Luteijn and Ketting 2013), which can include both a post-transcriptional component, by cleavage of target mRNAs, and a transcriptional component, by affecting chromatin at target loci (Pal-Bhadra et al., 2004; Kuramochi-Miyagawa et al., 2008; Sienski et al., 2012, 2015; Huang et al., 2013; Le Thomas et al., 2013; Manakov et al., 2015; Yu et al., 2015). Loss of piRNAs or PIWI proteins leads to elevated levels of transposon transcripts, increased double-strand breaks, meiotic arrest, and apoptosis of germ cells (Carmell et al., 2007; Houwing et al., 2007; Klattenhoff et al., 2007).

Even before the discovery of the piRNAs, PIWI proteins (for P-element Induced Wimpy testis) were known to have an important role in the stem cell biology of the *Drosophila* germline (Cox et al., 1998, 2000; Gonzalez et al., 2015). More recently, PIWI proteins have been reported outside of the gonads in various other stem cell systems and somatic tissues, including neuronal tissue, lung epithelium, intestine, fat body, the hematopoietic system, cardiac progenitors, and cancer cells (Sharma et al., 2001; Li et al., 2009a; Malone et al., 2009; Lee et al., 2011; Rajasethupathy et al., 2012; Perrat et al., 2013; Ortogero et al., 2014; Ross et al., 2014; Jones et al., 2016; Nandi et al., 2016; Vella et al., 2016; Sousa-Victor et al., 2017; Wasserman et al., 2017) and were detected broadly in somatic tissues of mollusks and arthropods (Jehn et al., 2018; Lewis et al., 2018), suggesting that in their ancestral state PIWI proteins were probably widely expressed and had functions independent of germline maintenance. However, reports on the presence of piRNAs and the relevance of PIWI in these tissues are at times conflicting (Nolde et al., 2013; Tosar et al., 2018; Genzor et al., 2019), and thus the biological role of the piRNA pathway in extra-gonadal tissues has remained ambiguous.

Somatic stem cells of highly regenerative animals, such as cnidarians, sponges, acoels, and planarians, contain high levels of PIWI protein (Reddien et al., 2005; De Mulder et al., 2009; Friedländer et al., 2009; Funayama et al., 2010; Shibata et al., 2010; Juliano et al., 2014; Lim et al., 2014; Praher et al., 2017), and loss of piRNAs or PIWI proteins from these somatic stem cells invariably leads to loss of the regenerative potential of the animal (Reddien et al., 2005; De Mulder et al., 2009; Rinkevich et al., 2010; Srivastava et al., 2014; van Wolfswinkel 2014; Shibata et al., 2016), indicating that they have an important function in stem cell biology. Regenerative organisms therefore form attractive and accessible models to delineate the somatic functions of the piRNA pathway.

The planarian *Schmidtea mediterranea* encodes three PIWI proteins (Reddien et al., 2005; Palakodeti et al., 2008). SMEDWI-3 is a putative homolog of *Drosophila* Ago-3, whereas SMEDWI-1 and SMEDWI-2 are more similar to each other than to the two primary PIWI clades (Figure 1A). All three planarian *piwi* genes are expressed in the stem cells (neoblasts) with little expression outside of this cell population (Figure S1A) (Reddien et al., 2005; Palakodeti et al., 2008), and RNAi-mediated knockdown of *smedwi-2* or *smedwi-3* leads to complete animal lethality preceded by a decline of the neoblast population (Figures S1C and S1D) (Reddien et al., 2005; Palakodeti et al., 2008). Intriguing results in two planarian systems suggested that PIWI proteins might affect cell differentiation (Reddien et al., 2005; Shibata et al., 2016); however, the mechanism behind this has remained unknown.

To examine the impact of the piRNA pathway in stem cell biology, we studied the role of the PIWI protein SMEDWI-2 in planarian stem cells and stem cell function. Remarkably, we find that the loss of SMEDWI-2 protein expression from the stem cells leads to different outcomes depending on the lineage into which the cells differentiate. We find that SMEDWI-2 is directly targeted to repetitive regions in the genome, and loss of SMEDWI-2 results in decreased H3K9 methylation at these loci. Once the affected cells exit the stem cell state and progress through cell differentiation, chromatin defects compromise the cell differentiation process: the resulting differentiated cells show an increase in transcription of tissue-specific transposable elements, as well as a decrease in the transcription of

typical cell-type-specific markers. Moreover, we find that the lineage-specific changes in chromatin accessibility that take place during wild-type cell differentiation similarly cause the desilencing of lineage-specific subsets of transposons, and that these are actively restrained by SMEDWI-2. Differentiating cells thus inevitably incur the risk for deregulation unless surveillance by SMEDWI-2 brings their chromatin back under control. We conclude that although SMEDWI-2 directly targets transposable elements, the implications of its regulatory function extend well beyond repetitive sequences, and that SMEDWI-2 is essential to escort cells through their chromatin transitions during the process of cell differentiation.

RESULTS

Transposon deregulation in *smedwi-2(RNAi)* animals is tissue specific

smedwi-2 is primarily expressed in the neoblasts (Reddien et al., 2005) (Figure S1A), but its protein product localizes to the nuclei of most planarian cells (Figures 1B and 1C; Figure S1B) (Zeng et al., 2013; Kim et al., 2019). We detected similar levels of SMEDWI-2 protein across all tissues and cell stages tested (Figure 1C; Figure S1B), indicating that although the bulk of SMEDWI-2 protein synthesis likely takes place in the neoblasts, planarian cells of all cell types retain this protein in their nucleus throughout their lifespan.

Previous work had suggested that although loss of SMEDWI-2 protein is lethal, the neoblasts of *smedwi-2(RNAi)* animals appeared to be unaffected (Reddien et al., 2005). Indeed, we confirmed that neoblasts remained mitotically active upon loss of SMEDWI-2 (Figures S1C–S1F). Gene expression in the neoblast population also remained largely unchanged, and derepression of transposons was minimal in the neoblasts (Figure 1D), whereas differentiated cells showed stronger increases in transposon levels.

Interestingly, fluorescent *in situ* hybridization (FISH) using several transposon probes revealed that each transposon showed a unique but highly reproducible spatial pattern in *smedwi-2(RNAi)* animals that appeared to be reminiscent of a tissue type (Figure 1E; Figure S1G) and did not significantly overlap in individual cells (Figure 1F). We further noticed that the expression of transposable elements was cell autonomous, and that within a tissue, only cells that lacked SMEDWI-2 protein expressed their specific transposons (Figure 1G; Figure S1H).

RNA sequencing (RNA-seq) of isolated tissues confirmed the tissue specificity of transposon desilencing (Figure 1H). Some transposons had larger fold changes in neoblasts than in differentiated cells but still had very low read counts, and highly expressed transposons were detected only outside the neoblast population. *Gypsy*-related long terminal repeat (LTR) transposons were particularly prone to activation, and many *Gypsy*-related transposon copies were uniquely deregulated in a specific tissue (Figures 1H and 1I; Figures S1J and S1K).

These findings are remarkable, as we had expected loss of SMEDWI-2 to lead to global loss of transposon repression. Even if only a subset of planarian cells or a subset of transposons would be affected, we had expected the same set of transposons to be expressed in each

deregulated cell. Instead, we found expression of cell-type-specific subsets of transposable elements, revealing unexpected heterogeneity.

Tissue-specific gene expression is deregulated in *smedwi-2(RNAi)*

Loss of SMEDWI-2 leads to widespread tissue failure (Figure 2A; Figure S2A), and we noticed that although RNA levels of many transposons were increased in each of the isolated tissues in *smedwi-2(RNAi)* samples, coding genes characteristic for each tissue were generally reduced in expression (Figure 2B). Using double FISH to inspect the relation between transposon expression and tissue identity, we found that cells expressing the intestinally enriched transposon *BURRO1* that were clearly embedded in the intestinal lining nevertheless no longer expressed the intestinal marker *madt-1* (Figure 2C), or other intestine-specific transcripts (Figure S2B), indicating that they are unlikely to be functional intestinal cells. We detected a similar lack of neuronal markers from cephalic ganglion cells expressing the neuronally enriched transposon *GLT2* in *smedwi-2(RNAi)* animals (Figure 2D).

A possible explanation for the finding that transposon-expressing cells no longer express tissue-specific markers is that these cells are damaged by the high levels of transposon activity. To address this, we first applied live/dead staining using propidium iodide (PI) and calcein on macerated *smedwi-2(RNAi)* animals to isolate only viable cells. Using FISH, we found that transposon-expressing cells remained present among the isolated live differentiated cells (Figure 2E). Next, we used staining for the DNA damage marker poly-ADP ribose to evaluate the state of the genomic DNA, and we found that the *smedwi-2(RNAi)* cells showed no signs of increased DNA damage relative to control cells (Figure 2F). Further, we saw no improvement of the *smedwi-2(RNAi)* phenotype upon treatment with RNAi against the highly abundant and active retrotransposon *BURRO1* or with reverse transcriptase inhibitors (Figures S2C and S2D), indicating that transposon activity and resulting DNA breaks are most likely not the cause of the observed defects in cell regulation.

Together this shows that differentiated cells that lack SMEDWI-2 protein show major defects in tissue-specific gene expression.

Smedwi-2(RNAi) cell deregulation develops during cell differentiation

To determine what causes this transcriptional deregulation of *smedwi-2(RNAi)* cells, we first determined the temporal development of the phenotype. A time course of mRNA expression revealed that *smedwi-2(RNAi)* animals were already distinct from controls at day 4 after the start of treatment and progressively diverged from the controls (Figure 2G). Changes in gene expression affected genes characteristic of multiple tissues and exacerbated overtime(Figure 2H). Genesignaturesof early differentiating cell types were particularly strongly reduced, suggesting the phenotype may start in these cells.

We next determined the delay between cell division and transposon expression by labeling newly dividing cells with bromodeoxyuridine (BrdU) and probing for co-expression with the transposon *GLT2* at different time points after labeling (Figure 2I; Figure S2E). The delay between S-phase and M-phase in the planarian cell cycle is estimated to be around 8

h (Newmark and Sánchez Alvarado, 2000); however, no overlap between BrdU-labeled cells and transposon expression was detected at 4 h or at 24 h after labeling. Only at 72 h after BrdU incorporation was *GLT2* expression detected in BrdU-labeled cells. This shows that deregulation of transposon expression happens not in cells that are actively cycling but rather in the early days after cell-cycle exit.

We further tracked the deregulation of *smedwi-2(RNAi)* cells by qPCR analysis of EdU pulse-labeled cells at different time points after their last division (Figure 2J). At 1 day after labeling, cells have started their differentiation trajectories, and early differentiation markers are highly expressed. Early epidermal markers *p53*, *prog-1*, and *prog-2* (Eisenhoffer et al., 2008; van Wolfswinkel et al., 2014) decreased rapidly after day 1 in both control and *smedwi-2(RNAi)* cells. In *smedwi-2(RNAi)* samples, however, expression of intermediate epidermal genes *agat-1*, *agat-2*, and *agat-3* was delayed, indicating that these cells proceed along an altered epidermal-like differentiation path. Similarly, early intestinal markers *nkx-2.2* and *hnf-4* (Forsthoefel et al., 2012; van Wolfswinkel et al., 2014) dropped rapidly in *smedwi-2(RNAi)* cells after 1 day of cell-cycle exit, but the increase in *gata-4/5/6* was delayed (Figure 2J). Whereas the late intestinal marker *madt-1* could just be detected toward the end of the time course in control cells, this stage was not reached in the *smedwi-2(RNAi)* differentiating cells. Importantly, we found no significant shift in the fraction of cells entering the epidermal lineage (Figure S2F), indicating that the detected RNA changes are due to expression changes in individual cells rather than changes in the number of cells in the lineages.

Taken together, these data indicate that *smedwi-2(RNAi)* affects the overall differentiation trajectories of newly differentiating cells resulting in altered gene expression and defective cell differentiation.

SMEDWI-2 targets genomic regions rich in transposon sequence

Although transposons are typical piRNA targets, studies across model systems have found large fractions of piRNAs that do not correspond to repetitive elements (Aravin et al., 2007; Houwing et al., 2007; Palakodeti et al., 2008; Friedländer et al., 2009; Kim et al., 2019), and several have suggested direct regulation of coding genes by PIWI proteins (Wu and Zamore 2021). Thus, the developmental defects in *smedwi-2(RNAi)* cells could be caused by the deregulation of targeted mRNAs.

To identify SMEDWI-2 targets, we immunoprecipitated SMEDWI-2 protein and analyzed the bound small RNAs (Figures S3A–S3C). The isolated RNAs had the length (31–35 nt) and 3′ methylation characteristic of piRNAs, indicating that the isolated small RNAs are genuine piRNA molecules. 49% of the SMEDWI-2-bound piRNAs mapped to annotated transposons (Figure 3A), a further 2.5% mapped to the non-repetitive transcriptome, and 43% mapped to the planarian genome, but not to any annotated elements. These genomic piRNAs were overwhelmingly derived from the same genomic regions as the transposon-related piRNAs (Figure 3B), indicating that their classification is most likely the result of incomplete annotation of planarian transposable elements. We therefore conclude that over 90% of the SMEDWI-2-bound piRNAs match repetitive regions.

Protein-coding genes made up only a minor fraction of SMEDWI-2 piRNAs, and several lines of evidence suggest that they are likely aspecific degradation remnants of mRNAs rather than regulatory RNAs: the majority of coding genes had very few matching piRNA reads (Figure 3C; Figure S3D); reads matching to coding genes were depleted from the SMEDWI-2 immunoprecipitation (IP) compared with the total small RNA pool (Figure 3D), and whereas transposon-related piRNAs were mostly antisense and therefore could target such sequences by base pairing, genic piRNAs were primarily in the sense orientation, which does not allow for any such effect (Figure S3E). Furthermore, we found a general correlation between mRNA abundance and genic piRNA read count, supporting the idea that the identified genic small RNAs could be remnants of regular mRNA metabolism. Finally, transposable elements, in particular LTR retrotransposons and polintons, showed clear evidence of piRNA-guided silencing by SMEDWI-2 (Figure 3E): elements with more piRNAs tended to show stronger de-repression upon *smedwi-2* knockdown (r = 0.63), whereas SMEDWI-2-bound genic piRNAs showed no correlation (r = 0.06) with effects of *smedwi-2(RNAi)* on genic transcript levels (Figure S3F), even when releasing the stringency of mapping to allow for base pairing limited to the "seed" region of the piRNA. Together this suggests that SMEDWI-2-bound piRNAs are unlikely to target protein-coding genes. Occasional genes that were nevertheless upregulated upon *smedwi-2* knockdown, and therefore could potentially be direct targets of SMEDWI-2-mediated repression, tended to have large amounts of transposon sequence in their surrounding non-coding regions (Figures S3G and S3H), suggesting that some of the observed genic changes are likely due to co-regulation with their genomic environment rather than to direct genic targeting by piRNAs, similar to what has been proposed before in *Drosophila* (Sienski et al., 2012). However, the majority of altered coding genes were downregulated upon loss of SMEDWI-2, suggesting a different mechanism of regulation. These genes did not show proximity of transposon sequences or coverage of piRNAs but tended to cluster together in genomic regions (see below).

Together these findings indicate that repetitive elements are the primary targets of SMEDWI-2-mediated regulation, and that direct targeting of coding genes is unlikely.

SMEDWI-2 controls chromatin accessibility at its targeted regions

PIWI proteins can exert their effect on the transcriptional or on the posttranscriptional level, and the nuclear localization of SMEDWI-2 suggests that it may well regulate gene expression at the transcriptional level.

To evaluate this, we performed the assay for transposase-accessible chromatin with sequencing (ATAC-seq) on neoblasts and differentiated cells from both wild-type animals and *smedwi-2(RNAi)* animals, and compared changes in chromatin accessibility with the genomic density of the cloned piRNA sequences (Figure 3F). We found that in both cell types, chromatin at loci with high levels of piRNAs became generally more accessible (higher ATAC-seq read coverage, p < 2.2e−16) upon *smedwi-2* knockdown, suggesting that SMEDWI-2 has a generally repressive effect on chromatin at its target loci. These loci overwhelmingly corresponded to transposon-rich regions. In contrast, loci with low

piRNA density, largely corresponding to genes, tended to show reduced accessibility in the *smedwi-2(RNAi)* animals.

To further investigate the chromatin organization in *smedwi-2* knockdown animals, we analyzed changes in activating (H3K4me3) (Kim et al., 2019) (Figure 3G) and repressive (H3K9me3) (Figure 3H) histone modifications in response to loss of SMEDWI-2 and related them to piRNA density. More than 90% of the altered H3K4me3 peaks at piRNA-targeted regions gained H3K4me3 signal, whereas more than 60% of the altered H3K9me3 peaks lost H3K9me3 signal, indicating that both marks contribute to the increased chromatin accessibility at the piRNA-targeted regions in *smedwi-2* knockdown animals. Moreover, peaks overlapping transposons were more likely to gain H3K4me3 and lose H3K9me3 signals, consistent with our observations that primarily transposon transcripts are upregulated upon *smedwi-2(RNAi)*.

Not all transposon families were affected equally. Transposons belonging to the LTR retrotransposons and Polintons, which had shown a clear correlation between piRNA density and the magnitude of transcript deregulation in *smedwi-2(RNAi)* animals (Figure 3E), also showed stronger effects at the chromatin level (Figures S3I–S3J).

Overall, we observed clear and consistent changes in the chromatin state of regions targeted by SMEDWI-2-bound piRNAs, indicating that SMEDWI-2 mediates repression of its direct targets (at least in part) at the chromatin level.

Transposons are reactivated by the cell differentiation process

But why is the desilencing of transposon regions upon loss of SMEDWI-2 tissue specific? This heterogeneity in outcome could either be caused by tissue-specific changes in SMEDWI-2 targeting or by tissue-specific differences in the activation potential of the transposons.

SMEDWI-2 remains present in the nuclei of differentiated cells (Figure 1C; Figure S1C) and remains loaded with piRNAs (Figure 4A), so differences in piRNA populations could explain differences in targeting. However, we found that the SMEDWI-2 piRNA populations in neoblasts, brain, epidermis, and intestine were highly similar (Figure 4B; Figure S4A). Even transposons with clear tissue-specific RNA expression upon *smedwi-2(RNAi)* showed no significant differences in piRNA levels, indicating that the tissue-specific effects are not due to tissue-specific targeting of SMEDWI-2.

We next focused on the chromatin state of the different cell types. Cell differentiation is accompanied by tissue-specific changes in chromatin organization, and we had noticed that the effects of SMEDWI-2 on chromatin state were more pronounced in differentiated cells than in neoblasts (Figure 4C). We therefore asked whether tissue-specific chromatin changes that take place during cell differentiation could underlie the tissue-specific transposon derepression upon loss of SMEDWI-2.

We isolated wild-type neoblasts, brain, and epidermis to determine the changes that occur during normal cell differentiation. The extent of chromatin change varied strongly between tissues (Figure 4D): changes in accessible chromatin in the epidermis involved as much as

27.2% of the total genome, but shifts in the neuronal lineages were much more modest (7.1%). Further, the wild-type tissues already showed tissue specificity in transposon levels (Figure 4E), and the larger chromatin changes in epidermal differentiation correlated with higher increases in transposon activation in this lineage (Figure 4G). Furthermore, although the significantly activated chromatin regions (>4-fold increase in H3K4me3) covered only small fractions of the total genome (5% of the genome in brain and 9.8% of the genome in epidermis), these regions contained the majority of all the activated transposons (53% of activated transposons in brain and 74% in epidermis) (Figure 4D), indicating a close correlation between cell differentiation-related chromatin changes and transposon activation. Interestingly, the same transposon classes that are most heavily targeted by piRNAs (LTR retrotransposons, Polintons, and to a lesser extent, non-LTR retrotransposons) demonstrated higher levels of H3K4me3 and RNA increases during normal differentiation (Figure 4F; Figure S4B), indicating that they are actively repressed by SMEDWI-2-dependent regulation. Together, this shows that even in the wild-type situation, transposons are a persistent sleeping threat to the cells that can be awakened by the chromatin remodeling events during cell differentiation.

Next, we determined which regions changed in chromatin state in response to *smedwi-2(RNAi)*. We found that the genomic locations of the *smedwi-2*-dependent transposon changes differed significantly between tissues (Figure 4H) and correlated with the tissue-specific regions that increase in accessibility during normal cell differentiation (Figure 4I): transposons located in regions that increased in H3K4me3 during differentiation were over four times more likely to show further increases in H3K4me3 upon loss of SMEDWI-2 than transposons located in other regions of the genome (Figures 4I and 4J; Figure S4C).

Together, these data suggest that the chromatin changes during cell differentiation create an environment in which specific transposons can become expressed, and that SMEDWI-2 functions to actively maintain silencing of these transposons during fate transitions.

Loss of SMEDWI-2 results in incompletely differentiated cells that negatively affect animal health

We previously showed that genes are not direct targets of SMEDWI-2-bound piRNAs, but tissue-specific gene expression is clearly affected in *smedwi-2(RNAi)* animals (Figure 2). This was also detected at the chromatin level: genes that should gain accessibility during wild-type cell differentiation remained less accessible in *smedwi-2(RNAi)*, whereas genes that should be condensed were likely to remain accessible (Figures 5A and 5B), suggesting that cells do not reach their fully differentiated state. It is important to note that these findings are based on cells isolated by their tissue-specific localization or function, requiring that they have taken on a major portion of their tissue-specific features. Cells that would not have progressed this far in their differentiation are not included in this analysis, and therefore the detected effects are likely an underestimation of the actual differentiation defects.

Interestingly, downregulated genes tended to be concentrated in the genome. Although only 0.2% of the genome was decreased in accessibility upon loss of SMEDWI-2, 73%

of genes with reduced H3K4me3 were located in these regions (Figure 5C). Genes with reduced expression also tended to occur in clusters, indicating that their genomic location is relevant for their altered expression (Figure 5D). Because these genes are not direct targets of piRNAs, this is suggestive of long-range chromatin effects, changing the expression of all genes located in particular genomic regions.

Among the genes with significantly altered chromatin were several lineage-specific transcription factors. For example, *nkx2.2* and *hnf4*, major transcription factors in the intestinal lineage (Forsthoefel et al., 2012; van Wolfswinkel et al., 2014), showed significantly reduced promoter accessibility upon *smedwi-2(RNAi)* (Figure 5E). In accordance, the mRNA levels of these factors were significantly decreased. Similarly, epidermal transcription factors *p53* and *zfp-1* (van Wolfswinkel et al., 2014) were downregulated in *smedwi-2(RNAi)* animals (Figure S5A). A reduction of such transcription factors will result in downstream effects on gene expression unrelated to direct SMEDWI-2 targeting.

We thus propose that the losses in tissue-specific gene expression in *smedwi2(RNAi)* animals likely originate at the chromatin level, and that the lack of activation of major transcription factors results in further deregulation of gene expression and cell differentiation.

smedwi2(RNAi) animals have a remarkably short lifespan (Reddien et al., 2005). In fact, we found that lethality of *smedwi-2(RNAi)* animals occurred well before that of animals without any stem cells as induced by irradiation (Figure S5B; Figure 5F) or RNAi-mediated knockdown of histones (Figure S5C), suggesting that the complete absence of novel cell differentiation is less detrimental to the animal than aberrantly differentiating *smedwi-2(RNAi)* cells. Indeed, reducing cell differentiation by RNAi against the master transcription factor *mex-3* (Zhu et al., 2015) led to a delay in transposon upregulation, as well as a significant delay in organismal mortality (Figures 5G and 5H, $p < 0.0001$) compared with *smedwi-2* alone.

Together, these data indicate that the loss of SMEDWI-2 leads to altered and incomplete cell differentiation in several lineages, and that the accumulation of such poorly differentiated cells likely leads to the observed lethality in *smedwi-2(RNAi)* animals.

Neoblasts have a double layer of protection against transposon activation

Our data demonstrate an important role for SMEDWI-2 in maintaining chromatin integrity in differentiating planarian cells. Remarkably, the neoblasts appear to be spared and do not show major defects in function or gene expression (Figure 1D; Figure S1), even though SMEDWI-2 is present in these cells. In contrast with differentiated cells, neoblasts also contain cytoplasmic PIWI proteins SMEDWI-1 and SMEDWI-3, which could form a second layer of transposon control at the post-transcriptional level. Indeed, neither single RNAi of *smedwi-2* nor *smedwi-1/3* double RNAi resulted in detectable expression of transposons within the neoblasts, but *smedwi-1/2/3* triple RNAi neoblasts showed significant transposon upregulation (Figure 6A; Figure S6A). Of note, this functional redundancy is independent of

ping-pong amplification of piRNAs, which would fail as soon as either of the PIWI proteins involved is depleted.

We found that transposon sequences in *smedwi-2(RNAi)* neoblasts already had reduced levels of H3K9me3 marks (Figures 6B and 6D), indicating that their silencing is indeed compromised. In differentiated tissues such as the brain, where SMEDWI-1 and SMEDWI-3 are no longer present, opened transposons showed significantly higher RNA fold changes in *smedwi-2(RNAi)* compared with unchanged loci (Figure 6C). However, in neoblasts due to the presence of a backup mechanism, RNA levels of transposons were independent of their chromatin changes (Figures 6C and 6D).

Our data thus indicate that the neoblasts have two layers of protection against activation of transposons: SMEDWI-2 coordinates silencing at the transcriptional level by increasing H3K9 methylation at transposon loci, and SMEDWI-1 and SMEDWI-3 eliminate leak-through transposon transcripts at the post-transcriptional level.

DISCUSSION

Planarians have impressive regenerative and homeostatic abilities that rely on the long-term maintenance of somatic pluripotent stem cells and the tight control of cell fate. This poses a unique opportunity to identify the regulatory strategies that are essential for effective regeneration and stem cell health.

Previous studies had shown that the planarian PIWI protein SMEDWI-2 is essential for regeneration and homeostasis and had proposed that its role is in neoblast descendants, because little effect could be detected in the functioning of the neoblasts themselves (Reddien et al., 2005; Palakodeti et al., 2008; Shibata et al., 2016). However, how and when this effect might be brought about and what the implications of SMEDWI-2-mediated regulation might be had remained unclear because affected cells appeared apoptotic and could not be analyzed further (Shibata et al., 2016), and the majority of the piRNAs that determine targeting of SMEDWI-2 could not be annotated (Kim et al., 2019). Furthermore, the SMEDWI-2 protein is found in neoblasts and other cells (Shibata et al., 2016; Kim et al., 2019), so why the phenotype would reveal itself only after exit from the stem cell compartment remained unclear.

In this study, we make the remarkable finding that the cellular deregulation associated with loss of SMEDWI-2 is tissue specific. Previous studies on the piRNA pathway have largely focused on regulation of the germ cells where only a single differentiation trajectory is present and thus no lineage-specific effects could be discerned. In planarians, where the neoblasts can differentiate into any of the organism's cell types, the lineage-specific aspect of SMEDWI-2 becomes apparent upon its loss: different transposons were desilenced in each tissue, and tissue-specific alterations in the expression of coding genes were detected. These differences between tissues were not caused by differences in SMEDWI-2 piRNAs, but rather by differences in the accessible chromatin regions in the cells, revealing a complex interplay between PIWI-mediated regulation of transposon regions and cell differentiation. This dimension of piRNA-mediated regulation is highly relevant for stem cell function. We

find that even during normal cell differentiation, the expression of transposons increases in a cell-type-specific way, and that this is correlated with the extent of the chromatin changes. SMEDWI-2 then functions to regain control of these regions (Figure 7). In the absence of SMEDWI-2, transposons located in genomic regions that gain accessibility during normal differentiation are further unleashed at the chromatin level. This leads to widespread effects on chromatin organization and interferes with the normal cell differentiation process. The differentiating *smedwi-2(RNAi)* cells do enter the cell differentiation trajectory but are unable to complete the chromatin transitions that accompany regular cell differentiation and do not activate cell-type-specific genes, including several transcription factors, leading to incompletely differentiated cells.

We find that SMEDWI-2 has a cell-autonomous function in the regulation of cell differentiation that is mediated through the establishment and maintenance of H3K9 methylation at repetitive elements (Figure 7). This proposed role of SMEDWI-2 in maintaining the repressed chromatin state of its target regions is in agreement with previous findings on the activities of nuclear PIWI proteins in mouse and *Drosophila* (Klenov et al., 2007; Wang and Elgin 2011; Sienski et al., 2012; Le Thomas et al., 2013; Rozhkov et al., 2013; Iwasaki et al., 2016). The nuclear PIWI proteins are not a monophyletic group (Figure 1A) (Lewis et al., 2016), and the only two well-characterized nuclear PIWIs (mouse and *Drosophila*) show significant divergence in the interacting proteins involved. Methylation of H3K9 is part of the silencing mechanism in both systems, and our findings now indicate further conservation of this aspect of PIWI-mediated regulation in planarians. In fact, in the neoblasts, the only detectable defect upon *smedwi-2(RNAi)* was at the chromatin of repetitive regions, providing strong indication that this lies at the basis of the later defects in these animals. Further analyses will reveal the direct effectors of this modification and may identify additional points of conservation between nuclear PIWI pathways.

Loss of PIWI proteins has been associated with upregulation of transposon transcripts, transposon jumping (Kalmykova et al., 2005; Jones et al., 2016), endoviral activity (Sarot et al., 2004; Shibata et al., 2016), meiotic arrest (Deng and Lin 2002; Kuramochi-Miyagawa et al., 2004), DNA damage (Klattenhoff et al., 2007; Khurana et al., 2010), chromatin changes (Brower-Toland et al., 2007; Klenov et al., 2007, 2011; Wang and Elgin 2011; Sienski et al., 2012), and apoptosis (Carmell et al., 2007; Houwing et al., 2007). It has been difficult to untangle the causal relationships between these effects in other model systems, but several lines of evidence argue that the cellular deregulation in planarian *smedwi-2(RNAi)* cells is caused by chromatin defects rather than other causes.

First, we did not find any evidence of infectious properties of *smedwi-2(RNAi)* animals (data not shown), and we found that effects of SMEDWI-2 loss were cell autonomous, arguing against viral intermediates. Second, treatment with broad reverse-transcriptase inhibitors did not improve the lifespan or phenotypic progression of the *smedwi-2(RNAi)* animals, arguing against the involvement of retrotransposon activity. Third, although *in situ* staining methods showed that loss of SMEDWI-2 leads to highly elevated expression of specific transposons in individual cells, RNAi-mediated knockdown of abundant transposons did not alter the phenotype or the progression of the *smedwi-2(RNAi)* animals, arguing against toxicity caused by abundant RNA intermediates. Moreover, we already detected

alterations in chromatin accessibility in the neoblasts, where no RNA-related phenotypes have yet developed. Fourth, no increase in DNA damage was detected in the affected cells, and cells with high levels of DNA damage, such as induced by irradiation or reactive oxygen species, do not show any of the cellular phenotypes of *smedwi-2(RNAi)* animals.

Together these findings support the altered chromatin state of the cells as the fundamental defect in the *smedwi-2(RNAi)* phenotype.

The role of PIWI in safeguarding chromatin transitions may hold relevance for many systems aside from planarian neoblasts. The progression from germline stem cell through meiosis to mature germ cell involves major shifts in chromatin organization, and rather than transposon activation, it may well be the misregulation of these chromatin changes that causes the observed developmental phenotypes (Zamudio et al., 2015). Furthermore, PIWI proteins have been reported in many somatic tissues, in particular in many types of cycling cell. Findings in several systems (Zhu et al., 2012; Jones et al., 2016; Sousa-Victor et al., 2017; Wasserman et al., 2017) are suggestive of a defect in cell differentiation, which could be caused by large-scale misregulation of chromatin, similar to what we found in this study.

Although chromatin changes were already detectable in the neoblasts, alterations in RNA levels were evident only in cells that had exited the neoblast state. We propose that there are two separate factors involved in this dichotomy. First, the transitions in cell fate coincide with tissue-specific changes in chromatin organization and thereby expose new transposons to a transcriptionally permissive environment. We found that transposons in newly opened regions of the genome had a high probability of becoming even more accessible in *smedwi-2(RNAi)* tissues, indicating that SMEDWI-2 functions to re-instate repression of transposons during and/or after the process of chromatin reorganization.

Second, our analysis revealed a backup mechanism composed of the cytoplasmic PIWI proteins SMEDWI-1 and SMEDWI-3, which are present only in the neoblasts (Figure 7). In the neoblasts, the loss of H3K9 methylation on transposon sequences does not lead to significant changes in transposon RNA levels because of the post-transcriptional control of these transcripts by the cytoplasmic PIWIs. Once that second protective layer is removed, either during normal cell differentiation or by *smedwi-1/3(RNAi)* in the neoblasts, transposon transcripts start to accumulate. This finding further shows that even though no obvious neoblast phenotype is detected at the level of cell function or RNA levels, SMEDWI-2 does confer protection against transposon expression in the neoblasts.

In conclusion, our findings provide a distinct perspective on the role of piRNAs in somatic cells and highlight the ongoing battle between repetitive elements and their host. Although transposons are often regarded as a threat to genetic integrity, our data show that during cell fate transitions transposons can also imperil the epigenetic integrity of the cell. PIWI proteins and piRNAs play a crucial role chaperoning the chromatin of planarian cells, and we expect that similar mechanisms will be in place in other multipotent stem cell systems to allow for their continued maintenance and control.

STAR★METHODS

RESOURCE AVAILABILITY

Lead contact—Requests for further information, resources, and reagents should be directed to and will be fulfilled by the Lead Contact, Dr. Josien van Wolfswinkel (Josien.van.wolfswinkel@yale.edu).

Materials availability—All unique reagents generated in this study are available from the Lead Contact with a completed Materials Transfer Agreement.

Data and code availability—All next generation sequencing data have been deposited at the SRA under the accession number PRJNA633618 and are publicly available as of the date of publication. Original western blot images and microscopy data will be shared by the lead contact upon request.

This paper does not report original code.

Any additional information required to reanalyze the data reported in this work is available from the Lead Contact upon request.

EXPERIMENTAL MODEL AND SUBJECT DETAILS

Schmidtea mediterranea asexual clonal strain ClW4 was maintained as previously described (Newmark and Sánchez Alvarado, 2000). Briefly, animals were cultured in 1x Montjuic salts at 20°C, fed homogenized beef liver paste every 1–2 weeks, and expanded through continuous cycles of amputation or fissioning and regeneration. Animals were starved 1–2 weeks prior to experiments. For some RNAi experiments, water was supplemented with 50ug/ml Gentamicin sulfate (VWR) to prevent bacterial growth.

METHOD DETAILS

RNAi and transposon inhibition—Regions of planarian genes 0.5–2kb in length were amplified from complementary DNA (cDNA) using sequence specific primers (Table S1) with adaptor sequences. The PCR product was cloned into the pGEM-T vector (Promega) and verified by Sanger sequencing. Both RNA strands were synthesized *in vitro* from PCR-generated forward and reverse templates with flanking T7 promoters (TAATACGACTCACTATAGG), and annealed by incubation at 37°C for 30min. The transcribed ssRNA as well as the final dsRNA product were verified by gel electrophoresis.

Animals were starved 1–2 weeks prior to RNAi experiments. RNAi food was prepared by mixing 2ul of generic food coloring, 2ul of dsRNA and 50ul of homogenized beef liver (Rouhana et al., 2013) and fed to animals in 3-day intervals. *smedwi-2(RNAi), smedwi-1 smedwi-2 smedwi-3(triple RNAi), smedwi-2 h2b (double RNAi)* or *smedwi-2 mex-3(double RNAi)* animals were fed twice (on day 0 and day 3), while *smedwi-1(RNAi), smedwi-3(RNAi), smedwi-1 smedwi-3(double RNAi)* animals were fed three times (on day 0, day 3 and day 6), unless noted otherwise. DsRNA matching *C. elegans* gene *unc-22* was used as a negative control. *smedwi-2(RNAi)* animals for RNA-seq, ATAC-seq, CUTnTAG and small RNA-seq are collected on day 7 unless noted otherwise. *smedwi-2(RNAi)* animals

used for FISH and concanavalin-A stainings in Figures 1, 2, and 6 were collected at the end point of their survival curve. End points were defined as the first day when epidermal lesions were observed in some of the animals in the batch. At this time, animals that had not yet developed epidermal lesions were collected for FISH. If left undisturbed, 100% of *smedwi-2(RNAi)* the animals will reach lethality within 2 days of the end point.

For transposon RNA inhibition, animals were fed control or *smedwi-2* dsRNA on day 0 and day 3. DsRNA matching transposon *BURRO1* was added into the same feed on day 3. For retrovirus inhibition, reverse transcriptase inhibitors azidothymidine (AZT, Cayman Chemical), lamivudine (3TC, Cayman Chemical) and stavudine (d4T, Cayman Chemical) were added to the same feed on day 3, at a final concentration of 1.6mM each.

Neoblast tracing using thymidine homologs—For BrdU pulse chase, control or *smedwi-2(RNAi)* animals were first fed with corresponding dsRNA in liver on day 0. On day 4, animals were treated with 0.06% N-acetyl cystine (NAC, Sigma) dissolved in 1x Montjuic salts for 1min, then soaked in 25mg/ml 5-bromo-2′-deoxyuridine (BrdU, Sigma) dissolved in 1x Montjuic salts containing 3% DMSO for 16h. Following BrdU pulse, animals were washed and chased in 5g/L Instant Ocean for 4h, 26h, or 76h. BrdU was detected by whole-mount immunofluorescence (see below).

For EdU labeling, control or *smedwi-2(RNAi)* animals were fed with liver containing corresponding dsRNA on day 0, and with liver containing dsRNA and 0.5mg/ml 2′S-2′-Deoxy-2′-fluoro-5-ethynylurie (F-ara-EdU, Sigma) on day 5. EdU was dissolved as 10x stock in 10% DMSO. At 20h, 44h, 68h and 92h after EdU feed, animals were sacrificed, and EdU labeled differentiating cells were detected using click-it reaction and isolated using FACS. Cell suspension was prepared following the FACS procedures described previously (van Wolfswinkel et al., 2014), fixed in 0.5% formaldehyde and stained with click-it solution (2mM $CuSO_4$, 2mM Sulfo-Cyanine3 azide (Lumiprobe, C1330), 20mg/ml Ascorbic Acid in PBS) for 30min at room temperature in dark. Following PBSB wash, cells were stained with DAPI, and the EdU positive population at G0/G1 phase was isolated by FACS. Cells were decrosslinked by incubating in 10mM EDTA, 0.1% SDS at 65°C for 2h, followed by proteaseK incubation at 55°C for 30min. RNA was extracted using TrizolLS (Invitrogen), treated with RQ1 DNase (Promega), reverse-transcribed using random hexamer (Invitrogen), and gene expression was assayed by qPCR.

Whole-mount fluorescent *in situ* hybridization—Fixations and whole-mount *in situ* hybridizations (ISH) were performed as previously described (Pearson et al., 2009), with alterations described in (King and Newmark 2013). Briefly, formaldehyde fixed animals were bleached using formamide bleach solution and treated with proteinase K (2 ug/ml) in PBSTx. Following overnight hybridization at 56°C, samples were washed sequentially in pre-hyb solution, 1:1 pre-hyb-2x SSC, 2x SSC and 0.2x SSC at 56°C. Probes were detected with anti-DIG-POD (Roche 11207733910), anti-Fl-POD (Roche 11426346910), or anti-DNP-HRP (Perkin Elmer PF1129). After tyramide development (King and Newmark 2013), peroxidase was inactivated by incubation in 1% sodium azide. Specimens were counterstained with DAPI (Sigma).

Expression and purification of SMEDWI-2 protein—The N-terminal domain of SMEDWI-2 protein (aa 1–166) was cloned into pET28 in front of a GST tag. Constructs were verified by Sanger sequencing, and transformed into *E. coli* strain BL21 for expression. SMEDWI-GST protein was purified using Pierce Glutathione Agarose (Thermo Scientific) following manufacturer's instruction. The GST tag was cleaved using PreScission Protease (GE Healthcare), and removed by passage over the glutathione column.

SMEDWI antibody generation—Protein antibody against SMEDWI-2 was generated by Cocalico Biologicals (Stevens, PA). The serum was purified using antigens immobilized on CNBr columns, as described by (Kavran and Leahy 2014). To eliminate cross-reactivity, antibody was negatively selected on column with *in vitro* expressed SMEDWI-1 N-terminal domain.

As a separate approach, peptide antibody was generated by immunization of rabbits with a peptide derived from the PAZ domain of SMEDWI-2, followed by affinity purification of the antibody from serum. All western blots and immunofluorescent stainings of SMEDWI-2 have been verified with both antibodies.

SDS-PAGE and western blotting—Individual 1–3mm sized animals were homogenized in protein loading buffer (60mM Tris-Cl pH6.8, 5% Glycerol, 1% SDS and 2.5% β-mercaptoethanol) and separated on 8% denaturing polyacrylamide gel. Samples were transferred to PVDF membrane, blocked, and incubated with the primary antibody in PBSTw containing 1.5% milk. The following commercial antibodies were used: mouse anti-α-tubulin (Millipore) at 1:10000; rabbit anti-GAPDH (Proteintech) at 1:3000, rabbit anti-Histone3 (Abcam) at 1:2000. Secondary antibodies goat anti-Rabbit IgG HRP Conjugate or goat anti-Mouse IgG HRP Conjugate (Life Technologies) were used at 1:10000 in PBSTw containing 1.5% milk.

Cell fractionation—10 1cm sized animals were dissociated as described previously (van Wolfswinkel et al., 2014). Single cell suspension of 1 million cells were dounced. Nuclei were precipitated by centrifuging at 1000 g for 10min, and the cytoplasmic and nuclear fractions were analyzed by western blot.

Whole-mount immunofluorescence—Animals were fixed as described above for FISH, bleached with methanol bleach solution, and permeabilized using with proteinase K (2 ug/ml) in PBSTx. Animals were blocked and incubated with primary antibody overnight, followed by incubation with goat anti-Rabbit IgG HRP Conjugate (Life Technologies) or goat anti-Mouse IgG HRP Conjugate (Life Technologies). Primary antibodies used were rabbit anti-phospho-Histone3[Ser10] (Millipore, clone 63–1C-8) 1:750, and mouse anti-BrdU (BD Biosciences) diluted 1:300. For BrdU labeling, samples were pretreated by incubation in 2N HCl (+0.5% Triton X-100) for 45 minutes followed by brief neutralization in 0.1M sodium borate. Signals were developed using Tyramide SuperBoost Kits (Invitrogen). Lectin stains were performed overnight at 4°C with fluorescein-conjugated lectin Concanavalin-A (Vector Labs). poly-ADP-ribose stains were performed on isolated cells as described previously (Tartier et al., 2003).

Planarian tissue isolations—Neoblasts in G2/M phase (X1), or G0/G1 phase (X2), and differentiated cells (Xins) were isolated by Fluorescence-Activated Cell Sorting based on DNA content (Hoechst fluorescence) as reported by (Hayashi et al., 2006), following the procedures described previously (van Wolfswinkel et al., 2014).

Planarian brains used for RNA-seq and small RNA pull down were isolated by fixation in 0.33N HCl and dissection as described by (Wang et al., 2016). Brains used for CUTnTAG were dissected from animals fixed in 2% formaldehyde in order to better preserve the chromatin.

Planarian pharynxes were isolated by treating the animals with 100mM NaAz, as described in (Shiroor et al., 2018).

Planarian intestinal cells were isolated using a protocol adapted from (Forsthoefel et al., 2012). Briefly, 125 ul of basic MACS beads (Miltenyi Biotech) were fed to large animals. After 48h, animals were dissociated as described previously (van Wolfswinkel et al., 2014), with the addition of 2mM EDTA to the dissociation buffer (CMFB-E). The cell suspension was flowed through a MACS LS column (Miltenyi Biotech), washed with CMFB-E for 3 times, and after removal from the magnet intestinal cells were eluted using 3×3ml ice cold CMFB-E. Cells were inspected and counted using a hemocytometer.

Planarian epidermis used for RNA-seq was isolated as described by (Wurtzel et al., 2017), with the alteration that 7.8% Ammonium Thiocyanate (Sigma-Aldrich) in PBS was used. Epidermal cells used for ATAC-seq, CUTnTAG and small RNA pull down were isolated based on the adhesive nature of these cells using MACS LS columns at low EDTA concentration (0.5mM).

The purity of all isolated tissues is confirmed by qPCR.

RNA-seq library generation—For mRNA-seq time course of neoblasts and total cells, 1000 neoblasts or 5000 total live cells were isolated by FACS from control or *smedwi(RNAi)* animals at corresponding time points. Libraries were generated by the SMARTseq2 protocol (Picelli et al., 2014).

For mRNA-seq libraries of bulk neoblasts and differentiated tissues, large animals were fed control *unc-22* or *smedwi-2* dsRNA in liver on day 0 and day 3, and sacrificed on day 6 (for epidermis isolation) or day 7 (for brain, pharynx, or intestinal isolation). Three biological replicates were analyzed for each tissue/treatment. RNA was extracted from isolated tissues using TRIzol Reagent (Invitrogen), and libraries were generated using TruSeq RNA Library Prep Kit v2 (Illumina) following manufacturer's instructions.

ATAC-seq library generation—For ATAC-seq libraries of G2/M phase neoblasts (X1), differentiated cells (Xins), epidermis, or intestine, large animals 1cm in length were fed with control *unc-22* or *smedwi-2* dsRNA in liver on day 0 and day 3, and sacrificed on day7. 100,000 neoblasts or differentiated cells, or 50,000 epidermal or intestinal cells were used for library generation. Three biological replicates were analyzed for each tissue/treatment.

Tn5 transposase was purified using the construct pTXB1-Tn5 (Addgene #60240) (Picelli et al., 2014). Transposase activity was verified by cleavage assay using linearized plasmid. ATAC-seq libraries were prepared as described in (Corces et al., 2017).

CUTnTAG library generation—For CUTnTAG libraries of G2/M phase neoblasts (X1), epidermal cells, or brain, large animals 1cm in length were fed control *unc-22* or *smedwi-2* dsRNA in liver on day 0 and day 3, and sacrificed on day7. Three biological replicates were analyzed for each tissue/treatment.

100,000 neoblasts or epidermal cells, or cells from 4 brains were permeabilized in NE1 buffer (20mM HEPS-KOH pH7.9, 10mM KCl, 0.5mM spermidine, 0.1% Triton X-100, and 20% glycerol) and fixed in 0.1% formaldehyde. Libraries were prepared as described in (Kaya-Okur et al., 2019). Primary antibodies rabbit anti-H3K4me3 (Millipore, 07–473) and rabbit anti-H3K9me3 (Abcam, AB8898) were used to detect histone modifications. Rabbit anti-GAPDH (Proteintech 10494-1-AP) was used as negative control. Secondary antibody Guinea pig anti-rabbit (novusbio, NBP1-72763) was used for all libraries.

Immunoprecipitation (IP) of SMEDWI-2—Starting material consisted of 10 million total cells, 1 million neoblasts (X1), 2 million mixed lineage differentiated cells (Xins), 400,000 epidermal cells, 800,000 intestinal cells, or 40 dissected brains from WT animals. Cells were lysed in RIPA lysis buffer supplemented with 5% glycerol, 0.3% Western Blot Buffer (Roche), and protease inhibitor (Roche)). 5% of the lysate was taken as input. Depending on the lysate, 0.25 – 1.25 ug of anti-SMEDWI-2 protein antibody and 5–25ul of Protein A magnetic beads (NEB) were added to the sample. Immunoprecipitation was performed following the NEB protocol. Small RNA was extracted using TRIzol.

Small RNA library generation—Following TRIzol extraction, IP or input small RNAs were further cleaned up either by eliminating longer RNAs using AmPure (Beckman Coulter), or by selecting for piRNAs with 3′ modifications using NaIO4 mediated oxidation (Vagin et al., 2006). Small RNA libraries were generated following a protocol adapted from the Zamore lab. Briefly, end-blocked, 5′ adenylated 3′ adaptor was ligated using T4 RNA Ligase 2, truncated KQ (NEB). Excess RT primer was added to anneal with the remaining 3′ adaptor, and 5′ adaptor was ligated using T4 RNA Ligase 1 (NEB). Reverse transcription was performed using AMV reverse transcriptase (NEB). PCR amplified libraries 144–158bp in size were selected by PAGE.

Microscopy and image analysis—Images were taken on a Zeiss LSM800 Confocal Microscope. Control and RNAi animals were imaged with the same magnification, laser intensity and gain, at comparable anatomical position. Images from representative single confocal planes are displayed in figures. Cell density quantification (Figure S2A) and colocalization analysis (Figures 2F, S1E, S1F, S1H, and S2D) were performed using the cell counter tool in Fiji (Schindelin et al., 2012). Cells were quantified across a 300um×300um field of view and z stack of 9 to 12 planes taken with 3um steps.

Processing of mRNA-seq data—mRNA libraries were sequenced on HiSeq 2500 or NovaSeq (Illumina). Reads were mapped against *Schmidtea mediterranea* transcriptomes

WIX1 (van Wolfswinkel et al., 2014), dd_Smed_v6 (Liu et al., 2013) or unigene (Robb et al., 2015) using Bowtie2 (Langmead and Salzberg 2012), and further processed with SAMtools (Li et al., 2009b). For transposon expression analysis, reads were mapped against the *Schmidtea mediterranea* SMESG.1 genome (Grohme et al., 2018) using STAR (Dobin et al., 2013). Genomic locations of transposon fragments were identified using RepeatMasker (Smit et al., 2013), based on consensus sequences in Repbase libraries (Bao et al., 2015).

To investigate tissue-specific expression and upregulation of transposons, RNaseq reads were mapped to individual transposon copies and ambiguously mapped reads were assigned to the most probable source using Telescope (Bendall et al., 2019). Transposon copies with a minimum average expression of 1 RPM per sample were filtered for differential expression analysis using DESeq2 (Love et al., 2014). Heatmap of the top 100 upregulated transposon copies per tissue upon *smedwi-2(RNAi)* (Figure 1H), or of all significantly upregulated transposon copies (Figure S1J) were plotted.

To investigate expression of tissue-specific genes, top 40 genes specific to each cell lineages were selected (Fincher et al., 2018; Plass et al., 2018) and their expression changes upon *smedwi-2(RNAi)* were plotted (Figure 2H). To obtain an overview of the gene expression changes in lineages (Figure 2B), a weighted vector of gene expression was calculated for each lineage based on data from (Fincher et al., 2018). Expression changes for each lineage were calculated by comparing total lineage expression in *smedwi-2(RNAi)* tissues to the control.

Processing of small RNA-seq data—Small RNA libraries were sequenced on NovaSeq, and 10–25M reads were generated for each sample. Following adaptor trimming by Cutadapt (Martin 2011), reads were mapped against the *Schmidtea mediterranea* SMESG.1 genome using Bowtie (Langmead 2010), allowing for 2 mismatches and up to 20 mapping locations. The reads are then counted strand-sensitively toward exons of transcripts or transposon copies using BEDTools.

To investigate targets of SMEDWI-2 associated piRNAs, adaptor trimmed reads were mapped sequentially against the following genomic sequences: *Schmidtea mediterranea* rRNA, tRNA, structural RNA, miRNA, transposons, the transcriptome and the genome. At each category, mapping with up to 2 mismatches allowed was attempted using Bowtie, mapped reads were excluded, and the rest of the library was used for mapping in the next category. Reads that were not accepted in any of the categories are marked as mapping to "none."

To investigate the genomic origin of SMEDWI-2 associated piRNAs, log10 RPM of piRNAs mapped perfectly and uniquely to the genome is plotted, along with transposon coverage per 10kb window (Figure 3B).

To investigate the density and directionality of SMEDWI-2 associated piRNAs over individual transcripts and transposon copies, piRNAs were mapped allowing for 2 mismatches and up to 20 possible locations. Among transcripts or transposon copies with at least 10 piRNAs mapped, those with forward piRNA bias are defined as ones with

more than 4 folds of forward-mapping piRNAs than reverse-mapping piRNAs. Those with strong forward piRNA bias are defines as ones with more than 10-folds of forward-mapping piRNAs than reverse-mapping piRNAs.

To investigate enrichment of SMEDWI-2 associated piRNAs over input, piRNAs from input or pull down libraries were mapped to individual transcripts and transposon copies, and the ratio between input and pull down piRNAs was calculated per transcript.

To investigate the relationship between piRNA count and transposon/transcript expression, piRNA were mapped to transposon consensus or transcripts, allowing up to 2 mismatches and randomly assigning multi-mappers to one of their best matching locations. Change of transposon/transcript expression in relationship to count of SMEDWI-2 associated piRNAs were plotted (Figures 3E and S3F).

Processing of ATAC-seq and CUTnTAG data—ATAC-seq and CUTnTAG libraries were sequenced on NovaSeq. We obtained at least 60M reads for each ATAC-seq sample and 3–10M reads for each CUTnTAG sample, as Kaya-Okur et al. (2019) has demonstrated that 3M reads are sufficient to capture the information in the low-background CUTnTAG libraries. Following adaptor trimming by Cutadapt (Martin 2011), reads were mapped against the concatenated sequence of the *Schmidtea mediterranea* chromosomal and mitochondrial genomes using Bowtie2, and further processed using SAMtools. PCR duplications were removed by Picard (https://broadinstitute.github.io/picard/). ATAC peaks were called using Genrich in ATAC-seq mode (https://github.com/jsh58/Genrich), and CUTnTAG peaks are called using MACS2 (Zhang et al., 2008; Gaspar 2018). Peaks were assigned to genomic features using BEDTools (Quinlan 2014). WIX1 transcripts with open reading frames that span > 50% of the transcript length and that blast to protein homologs in *C.elegans*, *Drosophila*, mice or human were defined as coding genes. Promoters were defined as 1 kb upstream and downstream of transcription start sites. Transposon loci were identified using RepeatMasker. Differential analysis of ATAC-seq or CUTnTAG peaks were performed using DiffBind (Stark and Brown, 2011) (Ross-Innes et al., 2012). Log2 fold change of ATAC-seq or CUTnTAG peaks upon *smedwi-2(RNAi)* in relationship to piRNA density over these peaks were plotted using ggplot2 (Wickham 2016) (Figures 3F–3H).

Chromatin state and expression profile analysis of transposons and coding genes—ATAC-seq, CUTnTAG, RNA-seq and small RNA-seq reads were mapped to the genome, and read counts over the exons of coding genes or transposon copies were obtained using HTseq (Anders et al., 2015), or BEDTools (Quinlan 2014). For small RNA reads, up to 2 mismatches and 10 possible genome locations were allowed. For other sequencing libraries, multi-mapping reads were randomly assigned to one of their best matching locations. Differential analysis of profile was performed using DESeq2. Changes of epigenetic profiles upon *smedwi-2* deficiency were analyzed by comparing *smedwi-2(RNAi)* samples to control ones (Figures 4D, 4H, 4I, and 5C). Changes during differentiation were analyzed by comparing control tissues with control neoblasts (Figures 4F, 4G, and 5A). Transposons and genes with chromatin state changes were defined as those with significant changes (p < 0.1) in one or more of the chromatin profiles (H3K4me3, H3K9me3 and ATAC).

Epigenetic profiles of specific genomic loci were visualized on IGV (Robinson et al., 2017), using reads combined from three replicates and normalized against the total millions of reads. Broad genomic view of epigenetic profiles (Figures 3B and 5D) was generated by summing up normalized reads over 10kb sliding genomic windows. Regions that open during differentiation (Figures 4D, 4I, 5B, and S4C) are identified as genomic windows that demonstrate 4 folds or higher normalized H3K4me3 profile in control differentiated tissue than control neoblasts. Regions that open upon *smedwi-2(RNAi)* (Figure 5C) are identified as genomic windows that demonstrate 2 folds or higher normalized H3K4me3 profile in *smedwi-2(RNAi)* sample than control. Transposon copies and genes within opening regions are identified using GRanges.

QUANTIFICATION AND STATISTICAL ANALYSIS

Levels of significance (Figures S1E, S1F, S2A, and S2F) were calculated with two-tailed Student's t test, using the Prism software package. Levels of significance for paired staining of control and treated cells (Figure 2F) were calculated using one-way ANOVA for matched measurements. Levels of significance for survival curves were calculated with Log-rank (Mantel-Cox) test, using the Prism software package. Analysis of genome-wide data was carried out as described above. The correlation coefficients were determined by Spearman's correlation, the fold enrichments were calculated using binomial test, the levels of significance for violin plots were calculated with Mann-Whitney U test, in the R software environment.

Supplementary Material

Refer to Web version on PubMed Central for supplementary material.

ACKNOWLEDGMENTS

REFERENCES

Anders S, Pyl PT, and Huber W (2015). HTSeq—a Python framework to work with high-throughput sequencing data. Bioinformatics 31, 166–169. [PubMed: 25260700]

Andrews S (2010). FastQC: A quality control tool for high throughput sequence data (Babraham Bioinformatics) https://www.bioinformatics.babraham.ac.uk/projects/fastqc/.

Aravin A, Gaidatzis D, Pfeffer S, Lagos-Quintana M, Landgraf P, Iovino N, Morris P, Brownstein MJ, Kuramochi-Miyagawa S, Nakano T, et al. (2006). A novel class of small RNAs bind to MILI protein in mouse testes. Nature 442, 203–207. [PubMed: 16751777]

Aravin AA, Sachidanandam R, Girard A, Fejes-Toth K, and Hannon GJ (2007). Developmentally regulated piRNA clusters implicate MILI in transposon control. Science 316, 744–747. [PubMed: 17446352]

Bao W, Kojima KK, and Kohany O (2015). Repbase Update, a database of repetitive elements in eukaryotic genomes. Mob. DNA 6, 11. [PubMed: 26045719]

Bendall ML, de Mulder M, Iñiguez LP, Lecanda-Sánchez A, Pérez-Losada M, Ostrowski MA, Jones RB, Mulder LCF, Reyes-Terán G, Crandall KA, et al. (2019). Telescope: Characterization of the retrotranscriptome by accurate estimation of transposable element expression. PLoS Comput. Biol 15, e1006453. [PubMed: 31568525]

Brennecke J, Aravin AA, Stark A, Dus M, Kellis M, Sachidanandam R, and Hannon GJ (2007). Discrete small RNA-generating loci as master regulators of transposon activity in Drosophila. Cell 128, 1089–1103. [PubMed: 17346786]

Brower-Toland B, Findley SD, Jiang L, Liu L, Yin H, Dus M, Zhou P, Elgin SC, and Lin H (2007). Drosophila PIWI associates with chromatin and interacts directly with HP1a. Genes Dev 21, 2300–2311. [PubMed: 17875665]

Carmell MA, Girard A, van de Kant HJ, Bourc'his D, Bestor TH, de Rooij DG, and Hannon GJ (2007). MIWI2 is essential for spermatogenesis and repression of transposons in the mouse male germline. Dev. Cell 12, 503–514. [PubMed: 17395546]

Corces MR, Trevino AE, Hamilton EG, Greenside PG, Sinnott-Armstrong NA, Vesuna S, Satpathy AT, Rubin AJ, Montine KS, Wu B, et al. (2017). An improved ATAC-seq protocol reduces background and enables interrogation of frozen tissues. Nat. Methods 14, 959–962. [PubMed: 28846090]

Cox DN, Chao A, Baker J, Chang L, Qiao D, and Lin H (1998). A novel class of evolutionarily conserved genes defined by piwi are essential for stem cell self-renewal. Genes Dev 12, 3715–3727. [PubMed: 9851978]

Cox DN, Chao A, and Lin H (2000). piwi encodes a nucleoplasmic factor whose activity modulates the number and division rate of germline stem cells. Development 127, 503–514. [PubMed: 10631171]

De Mulder K, Pfister D, Kuales G, Egger B, Salvenmoser W, Willems M, Steger J, Fauster K, Micura R, Borgonie G, and Ladurner P (2009). Stem cells are differentially regulated during development, regeneration and homeostasis in flatworms. Dev. Biol 334, 198–212. [PubMed: 19631639]

Deng W, and Lin H (2002). miwi, a murine homolog of piwi, encodes a cytoplasmic protein essential for spermatogenesis. Dev. Cell 2, 819–830. [PubMed: 12062093]

Dobin A, Davis CA, Schlesinger F, Drenkow J, Zaleski C, Jha S, Batut P, Chaisson M, and Gingeras TR (2013). STAR: ultrafast universal RNA-seq aligner. Bioinformatics 29, 15–21. [PubMed: 23104886]

Eisenhoffer GT, Kang H, and Sánchez Alvarado A (2008). Molecular analysis of stem cells and their descendants during cell turnover and regeneration in the planarian Schmidtea mediterranea. Cell Stem Cell 3, 327–339. [PubMed: 18786419]

Fincher CT, Wurtzel O, de Hoog T, Kravarik KM, and Reddien PW (2018). Cell type transcriptome atlas for the planarian Schmidtea mediterranea. Science 360, eaaq1736.

Forsthoefel DJ, James NP, Escobar DJ, Stary JM, Vieira AP, Waters FA, and Newmark PA (2012). An RNAi screen reveals intestinal regulators of branching morphogenesis, differentiation, and stem cell proliferation in planarians. Dev. Cell 23, 691–704. [PubMed: 23079596]

Friedländer MR, Adamidi C, Han T, Lebedeva S, Isenbarger TA, Hirst M, Marra M, Nusbaum C, Lee WL, Jenkin JC, et al. (2009). High-resolution profiling and discovery of planarian small RNAs. Proc. Natl. Acad. Sci. USA 106, 11546–11551. [PubMed: 19564616]

Funayama N, Nakatsukasa M, Mohri K, Masuda Y, and Agata K (2010). Piwi expression in archeocytes and choanocytes in demosponges: insights into the stem cell system in demosponges. Evol. Dev 12, 275–287. [PubMed: 20565538]

Gaspar JM (2018). Improved peak-calling with MACS2. bioRxiv 10.1101/496521.

Genzor P, Cordts SC, Bokil NV, and Haase AD (2019). Aberrant expression of select piRNA-pathway genes does not reactivate piRNA silencing in cancer cells. Proc. Natl. Acad. Sci. USA 116, 11111–11112. [PubMed: 31110013]

Girard A, Sachidanandam R, Hannon GJ, and Carmell MA (2006). A germline-specific class of small RNAs binds mammalian Piwi proteins. Nature 442, 199–202. [PubMed: 16751776]

Gonzalez J, Qi H, Liu N, and Lin H (2015). Piwi Is a Key Regulator of Both Somatic and Germline Stem Cells in the Drosophila Testis. Cell Rep 12, 150–161. [PubMed: 26119740]

Grivna ST, Beyret E, Wang Z, and Lin H (2006). A novel class of small RNAs in mouse spermatogenic cells. Genes Dev 20, 1709–1714. [PubMed: 16766680]

Grohme MA, Schloissnig S, Rozanski A, Pippel M, Young GR, Winkler S, Brandl H, Henry I, Dahl A, Powell S, et al. (2018). The genome of Schmidtea mediterranea and the evolution of core cellular mechanisms. Nature 554, 56–61. [PubMed: 29364871]

Hayashi T, Asami M, Higuchi S, Shibata N, and Agata K (2006). Isolation of planarian X-ray-sensitive stem cells by fluorescence-activated cell sorting. Dev. Growth Differ 48, 371–380. [PubMed: 16872450]

Houwing S, Kamminga LM, Berezikov E, Cronembold D, Girard A, van den Elst H, Filippov DV, Blaser H, Raz E, Moens CB, et al. (2007). A role for Piwi and piRNAs in germ cell maintenance and transposon silencing in Zebrafish. Cell 129, 69–82. [PubMed: 17418787]

Huang XA, Yin H, Sweeney S, Raha D, Snyder M, and Lin H (2013). A major epigenetic programming mechanism guided by piRNAs. Dev. Cell 24, 502–516. [PubMed: 23434410]

Iwasaki YW, Murano K, Ishizu H, Shibuya A, Iyoda Y, Siomi MC, Siomi H, and Saito K (2016). Piwi Modulates Chromatin Accessibility by Regulating Multiple Factors Including Histone H1 to Repress Transposons. Mol. Cell 63, 408–419. [PubMed: 27425411]

Jehn J, Gebert D, Pipilescu F, Stern S, Kiefer JST, Hewel C, and Rosenkranz D (2018). *PIWI* genes and piRNAs are ubiquitously expressed in mollusks and show patterns of lineage-specific adaptation. Commun. Biol 1, 137. [PubMed: 30272016]

Jones BC, Wood JG, Chang C, Tam AD, Franklin MJ, Siegel ER, and Helfand SL (2016). A somatic piRNA pathway in the Drosophila fat body ensures metabolic homeostasis and normal lifespan. Nat. Commun 7, 13856. [PubMed: 28000665]

Juliano CE, Reich A, Liu N, Götzfried J, Zhong M, Uman S, Reenan RA, Wessel GM, Steele RE, and Lin H (2014). PIWI proteins and PIWI-interacting RNAs function in Hydra somatic stem cells. Proc. Natl. Acad. Sci. USA 111, 337–342. [PubMed: 24367095]

Kalmykova AI, Klenov MS, and Gvozdev VA (2005). Argonaute protein PIWI controls mobilization of retrotransposons in the Drosophila male germline. Nucleic Acids Res 33, 2052–2059. [PubMed: 15817569]

Kavran JM, and Leahy DJ (2014). Coupling antibody to cyanogen bromide-activated sepharose. Methods Enzymol 541, 27–34. [PubMed: 24674060]

Kaya-Okur HS, Wu SJ, Codomo CA, Pledger ES, Bryson TD, Henikoff JG, Ahmad K, and Henikoff S (2019). CUT&Tag for efficient epigenomic profiling of small samples and single cells. Nat. Commun 10, 1930. [PubMed: 31036827]

Khurana JS, Xu J, Weng Z, and Theurkauf WE (2010). Distinct functions for the Drosophila piRNA pathway in genome maintenance and telomere protection. PLoS Genet 6, e1001246. [PubMed: 21179579]

Kim IV, Duncan EM, Ross EJ, Gorbovytska V, Nowotarski SH, Elliott SA, Sánchez Alvarado A, and Kuhn CD (2019). Planarians recruit piRNAs for mRNA turnover in adult stem cells. Genes Dev 33, 1575–1590. [PubMed: 31537626]

King RS, and Newmark PA (2013). In situ hybridization protocol for enhanced detection of gene expression in the planarian Schmidtea mediterranea. BMC Dev. Biol 13, 8. [PubMed: 23497040]

Klattenhoff C, Bratu DP, McGinnis-Schultz N, Koppetsch BS, Cook HA, and Theurkauf WE (2007). Drosophila rasiRNA pathway mutations disrupt embryonic axis specification through activation of an ATR/Chk2 DNA damage response. Dev. Cell 12, 45–55. [PubMed: 17199040]

Klenov MS, Lavrov SA, Stolyarenko AD, Ryazansky SS, Aravin AA, Tuschl T, and Gvozdev VA (2007). Repeat-associated siRNAs cause chromatin silencing of retrotransposons in the Drosophila melanogaster germline. Nucleic Acids Res 35, 5430–5438. [PubMed: 17702759]

Klenov MS, Sokolova OA, Yakushev EY, Stolyarenko AD, Mikhaleva EA, Lavrov SA, and Gvozdev VA (2011). Separation of stem cell maintenance and transposon silencing functions of Piwi protein. Proc. Natl. Acad. Sci. USA 108, 18760–18765. [PubMed: 22065765]

Kuramochi-Miyagawa S, Kimura T, Ijiri TW, Isobe T, Asada N, Fujita Y, Ikawa M, Iwai N, Okabe M, Deng W, et al. (2004). Mili, a mammalian member of piwi family gene, is essential for spermatogenesis. Development 131, 839–849. [PubMed: 14736746]

Kuramochi-Miyagawa S, Watanabe T, Gotoh K, Totoki Y, Toyoda A, Ikawa M, Asada N, Kojima K, Yamaguchi Y, Ijiri TW, et al. (2008). DNA methylation of retrotransposon genes is regulated by

Piwi family members MILI and MIWI2 in murine fetal testes. Genes Dev 22, 908–917. [PubMed: 18381894]

Langmead B (2010). Aligning short sequencing reads with Bowtie. Curr. Protoc. Bioinform 11, 11.7.1–11.7.14.

Langmead B, and Salzberg SL (2012). Fast gapped-read alignment with Bowtie 2. Nat. Methods 9, 357–359. [PubMed: 22388286]

Le Thomas A, Rogers AK, Webster A, Marinov GK, Liao SE, Perkins EM, Hur JK, Aravin AA, and Tóth KF (2013). Piwi induces piRNA-guided transcriptional silencing and establishment of a repressive chromatin state. Genes Dev 27, 390–399. [PubMed: 23392610]

Lee EJ, Banerjee S, Zhou H, Jammalamadaka A, Arcila M, Manjunath BS, and Kosik KS (2011). Identification of piRNAs in the central nervous system. RNA 17, 1090–1099. [PubMed: 21515829]

Lewis SH, Salmela H, and Obbard DJ (2016). Duplication and Diversification of Dipteran Argonaute Genes, and the Evolutionary Divergence of Piwi and Aubergine. Genome Biol. Evol 8, 507–518. [PubMed: 26868596]

Lewis SH, Quarles KA, Yang Y, Tanguy M, Frézal L, Smith SA, Sharma PP, Cordaux R, Gilbert C, Giraud I, et al. (2018). Pan-arthropod analysis reveals somatic piRNAs as an ancestral defence against transposable elements. Nat. Ecol. Evol 2, 174–181. [PubMed: 29203920]

Li C, Vagin VV, Lee S, Xu J, Ma S, Xi H, Seitz H, Horwich MD, Syrzycka M, Honda BM, et al. (2009a). Collapse of germline piRNAs in the absence of Argonaute3 reveals somatic piRNAs in flies. Cell 137, 509–521. [PubMed: 19395009]

Li H, Handsaker B, Wysoker A, Fennell T, Ruan J, Homer N, Marth G, Abecasis G, and Durbin R; 1000 Genome Project Data Processing Subgroup (2009b). The Sequence Alignment/Map format and SAMtools. Bioinformatics 25, 2078–2079. [PubMed: 19505943]

Lim RS, Anand A, Nishimiya-Fujisawa C, Kobayashi S, and Kai T (2014). Analysis of Hydra PIWI proteins and piRNAs uncover early evolutionary origins of the piRNA pathway. Dev. Biol 386, 237–251. [PubMed: 24355748]

Liu SY, Selck C, Friedrich B, Lutz R, Vila-Farré M, Dahl A, Brandl H, Lakshmanaperumal N, Henry I, and Rink JC (2013). Reactivating head re-growth in a regeneration-deficient planarian species. Nature 500, 81–84. [PubMed: 23883932]

Love MI, Huber W, and Anders S (2014). Moderated estimation of fold change and dispersion for RNA-seq data with DESeq2. Genome Biol 15, 550. [PubMed: 25516281]

Luteijn MJ, and Ketting RF (2013). PIWI-interacting RNAs: from generation to transgenerational epigenetics. Nat. Rev. Genet 14, 523–534. [PubMed: 23797853]

Malone CD, Brennecke J, Dus M, Stark A, McCombie WR, Sachidanandam R, and Hannon GJ (2009). Specialized piRNA pathways act in germline and somatic tissues of the Drosophila ovary. Cell 137, 522–535. [PubMed: 19395010]

Manakov SA, Pezic D, Marinov GK, Pastor WA, Sachidanandam R, and Aravin AA (2015). MIWI2 and MILI Have Differential Effects on piRNA Biogenesis and DNA Methylation. Cell Rep 12, 1234–1243. [PubMed: 26279574]

Martin M (2011). Cutadapt removes adapter sequences from high-throughput sequencing reads. EMBnet.Journal 17, 10–12.

Nandi S, Chandramohan D, Fioriti L, Melnick AM, Hébert JM, Mason CE, Rajasethupathy P, and Kandel ER (2016). Roles for small noncoding RNAs in silencing of retrotransposons in the mammalian brain. Proc. Natl. Acad. Sci. USA 113, 12697–12702. [PubMed: 27791114]

Newmark PA, and Sánchez Alvarado A (2000). Bromodeoxyuridine specifically labels the regenerative stem cells of planarians. Dev. Biol 220, 142–153. [PubMed: 10753506]

Nolde MJ, Cheng EC, Guo S, and Lin H (2013). Piwi genes are dispensable for normal hematopoiesis in mice. PLoS ONE 8, e71950. [PubMed: 24058407]

Ortogero N, Schuster AS, Oliver DK, Riordan CR, Hong AS, Hennig GW, Luong D, Bao J, Bhetwal BP, Ro S, et al. (2014). A novel class of somatic small RNAs similar to germ cell pachytene PIWI-interacting small RNAs. J. Biol. Chem 289, 32824–32834. [PubMed: 25320077]

Pal-Bhadra M, Leibovitch BA, Gandhi SG, Chikka MR, Bhadra U, Birchler JA, and Elgin SC (2004). Heterochromatic silencing and HP1 localization in Drosophila are dependent on the RNAi machinery. Science 303, 669–672. [PubMed: 14752161]

Palakodeti D, Smielewska M, Lu YC, Yeo GW, and Graveley BR (2008). The PIWI proteins SMEDWI-2 and SMEDWI-3 are required for stem cell function and piRNA expression in planarians. RNA 14, 1174–1186. [PubMed: 18456843]

Pearson BJ, Eisenhoffer GT, Gurley KA, Rink JC, Miller DE, and Sánchez Alvarado A (2009). Formaldehyde-based whole-mount *in situ* hybridization method for planarians. Dev. Dyn 238, 443–450. [PubMed: 19161223]

Perrat PN, DasGupta S, Wang J, Theurkauf W, Weng Z, Rosbash M, and Waddell S (2013). Transposition-driven genomic heterogeneity in the Drosophila brain. Science 340, 91–95. [PubMed: 23559253]

Picelli S, Faridani OR, Björklund AK, Winberg G, Sagasser S, and Sandberg R (2014). Full-length RNA-seq from single cells using Smartseq2. Nat. Protoc 9, 171–181. [PubMed: 24385147]

Plass M, Solana J, Wolf FA, Ayoub S, Misios A, GlaŽar P, Obermayer B, Theis FJ, Kocks C, and Rajewsky N (2018). Cell type atlas and lineage tree of a whole complex animal by single-cell transcriptomics. Science 360, eaaq1723.

Praher D, Zimmermann B, Genikhovich G, Columbus-Shenkar Y, Mode-palli V, Aharoni R, Moran Y, and Technau U (2017). Characterization of the piRNA pathway during development of the sea anemone Nematostella vectensis. RNA Biol 14, 1727–1741. [PubMed: 28783426]

Quinlan AR (2014). BEDTools: The Swiss-Army Tool for Genome Feature Analysis. Curr. Protoc. Bioinform 47, 11.12.1–11.12.34.

Rajasethupathy P, Antonov I, Sheridan R, Frey S, Sander C, Tuschl T, and Kandel ER (2012). A role for neuronal piRNAs in the epigenetic control of memory-related synaptic plasticity. Cell 149, 693–707. [PubMed: 22541438]

Reddien PW, Oviedo NJ, Jennings JR, Jenkin JC, and Sánchez Alvarado A (2005). SMEDWI-2 is a PIWI-like protein that regulates planarian stem cells. Science 310, 1327–1330. [PubMed: 16311336]

Rinkevich Y, Rosner A, Rabinowitz C, Lapidot Z, Moiseeva E, and Rinkevich B (2010). Piwi positive cells that line the vasculature epithelium, underlie whole body regeneration in a basal chordate. Dev. Biol 345, 94–104. [PubMed: 20553710]

Robb SM, Gotting K, Ross E, and Sánchez Alvarado A (2015). SmedGD 2.0: The Schmidtea mediterranea genome database. Genesis 53, 535–546. [PubMed: 26138588]

Robinson JT, Thorvaldsdóttir H, Wenger AM, Zehir A, and Mesirov JP (2017). Variant review with the integrative genomics viewer. Cancer Res 77, e31–e34. [PubMed: 29092934]

Ross RJ, Weiner MM, and Lin H (2014). PIWI proteins and PIWI-interacting RNAs in the soma. Nature 505, 353–359. [PubMed: 24429634]

Ross-Innes CS, Stark R, Teschendorff AE, Holmes KA, Ali HR, Dunning MJ, Brown GD, Gojis O, Ellis IO, Green AR, et al. (2012). Differential oestrogen receptor binding is associated with clinical outcome in breast cancer. Nature 481, 389–393. [PubMed: 22217937]

Rouhana L, Weiss JA, Forsthoefel DJ, Lee H, King RS, Inoue T, Shibata N, Agata K, and Newmark PA (2013). RNA interference by feeding in vitro-synthesized double-stranded RNA to planarians: methodology and dynamics. Dev. Dyn 242, 718–730. [PubMed: 23441014]

Rozhkov NV, Hammell M, and Hannon GJ (2013). Multiple roles for Piwi in silencing Drosophila transposons. Genes Dev 27, 400–412. [PubMed: 23392609]

Sarot E, Payen-Groschêne G, Bucheton A, and Pélisson A (2004). Evidence for a piwi-dependent RNA silencing of the gypsy endogenous retrovirus by the Drosophila melanogaster flamenco gene. Genetics 166, 1313–1321. [PubMed: 15082550]

Schindelin J, Arganda-Carreras I, Frise E, Kaynig V, Longair M, Pietzsch T, Preibisch S, Rueden C, Saalfeld S, Schmid B, et al. (2012). Fiji: an open-source platform for biological-image analysis. Nat. Methods 9, 676–682. [PubMed: 22743772]

Sharma AK, Nelson MC, Brandt JE, Wessman M, Mahmud N, Weller KP, and Hoffman R (2001). Human CD34(+) stem cells express the hiwi gene, a human homologue of the Drosophila gene piwi. Blood 97, 426–434. [PubMed: 11154219]

Shibata N, Rouhana L, and Agata K (2010). Cellular and molecular dissection of pluripotent adult somatic stem cells in planarians. Dev. Growth Differ 52, 27–41. [PubMed: 20078652]

Shibata N, Kashima M, Ishiko T, Nishimura O, Rouhana L, Misaki K, Yonemura S, Saito K, Siomi H, Siomi MC, and Agata K (2016). Inheritance of a Nuclear PIWI from Pluripotent Stem Cells by Somatic Descendants Ensures Differentiation by Silencing Transposons in Planarian. Dev. Cell 37, 226–237. [PubMed: 27165555]

Shiroor DA, Bohr TE, and Adler CE (2018). Chemical Amputation and Regeneration of the Pharynx in the Planarian Schmidtea mediterranea. J. Vis. Exp 2018, 57168.

Shore S, Henderson JM, Lebedev A, Salcedo MP, Zon G, McCaffrey AP, Paul N, and Hogrefe RI (2016). Small RNA Library Preparation Method for Next-Generation Sequencing Using Chemical Modifications to Prevent Adapter Dimer Formation. PLoS ONE 11, e0167009. [PubMed: 27875576]

Sienski G, Dönertas D, and Brennecke J (2012). Transcriptional silencing of transposons by Piwi and maelstrom and its impact on chromatin state and gene expression. Cell 151, 964–980. [PubMed: 23159368]

Sienski G, Batki J, Senti KA, Dönertas D, Tirian L, Meixner K, and Brennecke J (2015). Silencio/CG9754 connects the Piwi-piRNA complex to the cellular heterochromatin machinery. Genes Dev 29, 2258–2271. [PubMed: 26494711]

Smit A, Hubley R, Green P, 2013–2015. RepeatMasker Open-4.0 http://www.repeatmasker.org.

Sousa-Victor P, Ayyaz A, Hayashi R, Qi Y, Madden DT, Lunyak VV, and Jasper H (2017). Piwi Is Required to Limit Exhaustion of Aging Somatic Stem Cells. Cell Rep 20, 2527–2537. [PubMed: 28903034]

Srivastava M, Mazza-Curll KL, van Wolfswinkel JC, and Reddien PW (2014). Whole-body acoel regeneration is controlled by Wnt and Bmp-Admp signaling. Curr. Biol 24, 1107–1113. [PubMed: 24768051]

Stark R, and Brown G (2011). DiffBind: differential binding analysis of ChIP-Seq peak data http://bioconductor.org/packages/release/bioc/vignettes/DiffBind/inst/doc/DiffBind.pdf.

Tartier L, Spenlehauer C, Newman HC, Folkard M, Prise KM, Michael BD, Ménissier-de Murcia J, and de Murcia G (2003). Local DNA damage by proton microbeam irradiation induces poly(ADP-ribose) synthesis in mammalian cells. Mutagenesis 18, 411–416. [PubMed: 12960408]

Tosar JP, Rovira C, and Cayota A (2018). Non-coding RNA fragments account for the majority of annotated piRNAs expressed in somatic non-gonadal tissues. Commun. Biol 1, 2. [PubMed: 30271890]

Vagin VV, Sigova A, Li C, Seitz H, Gvozdev V, and Zamore PD (2006). A distinct small RNA pathway silences selfish genetic elements in the germline. Science 313, 320–324. [PubMed: 16809489]

van Wolfswinkel JC (2014). Piwi and potency: PIWI proteins in animal stem cells and regeneration. Integr. Comp. Biol 54, 700–713. [PubMed: 24948137]

van Wolfswinkel JC, Wagner DE, and Reddien PW (2014). Single-cell analysis reveals functionally distinct classes within the planarian stem cell compartment. Cell Stem Cell 15, 326–339. [PubMed: 25017721]

Vella S, Gallo A, Lo Nigro A, Galvagno D, Raffa GM, Pilato M, and Conaldi PG (2016). PIWI-interacting RNA (piRNA) signatures in human cardiac progenitor cells. Int. J. Biochem. Cell Biol 76, 1–11. [PubMed: 27131603]

Wang SH, and Elgin SC (2011). Drosophila Piwi functions downstream of piRNA production mediating a chromatin-based transposon silencing mechanism in female germ line. Proc. Natl. Acad. Sci. USA 108, 21164–21169. [PubMed: 22160707]

Wang IE, Lapan SW, Scimone ML, Clandinin TR, and Reddien PW (2016). Hedgehog signaling regulates gene expression in planarian glia. eLife 5, e16996. [PubMed: 27612382]

Wasserman GA, Szymaniak AD, Hinds AC, Yamamoto K, Kamata H, Smith NM, Hilliard KL, Carrieri C, Labadorf AT, Quinton LJ, et al. (2017). Expression of Piwi protein MIWI2 defines a distinct population of multi-ciliated cells. J. Clin. Invest 127, 3866–3876. [PubMed: 28920925]

Wickham H (2016). ggplot2: Elegant Graphics for Data Analysis (Springer-Verlag New York).

Wu PH, and Zamore PD (2021). Defining the functions of PIWI-interacting RNAs. Nat. Rev. Mol. Cell Biol 22, 239–240. [PubMed: 33483697]

Wurtzel O, Oderberg IM, and Reddien PW (2017). Planarian Epidermal Stem Cells Respond to Positional Cues to Promote Cell-Type Diversity. Dev. Cell 40, 491–504.e5. [PubMed: 28292427]

Yu Y, Gu J, Jin Y, Luo Y, Preall JB, Ma J, Czech B, and Hannon GJ (2015). Panoramix enforces piRNA-dependent cotranscriptional silencing. Science 350, 339–342. [PubMed: 26472911]

Zamudio N, Barau J, Teissandier A, Walter M, Borsos M, Servant N, and Bourc'his D (2015). DNA methylation restrains transposons from adopting a chromatin signature permissive for meiotic recombination. Genes Dev 29, 1256–1270. [PubMed: 26109049]

Zeng A, Li YQ, Wang C, Han XS, Li G, Wang JY, Li DS, Qin YW, Shi Y, Brewer G, and Jing Q (2013). Heterochromatin protein 1 promotes self-renewal and triggers regenerative proliferation in adult stem cells. J. Cell Biol 201, 409–425. [PubMed: 23629965]

Zhang Y, Liu T, Meyer CA, Eeckhoute J, Johnson DS, Bernstein BE, Nusbaum C, Myers RM, Brown M, Li W, and Liu XS (2008). Model-based analysis of ChIP-Seq (MACS). Genome Biol 9, R137. [PubMed: 18798982]

Zhu W, Pao GM, Satoh A, Cummings G, Monaghan JR, Harkins TT, Bryant SV, Randal Voss S, Gardiner DM, and Hunter T (2012). Activation of germline-specific genes is required for limb regeneration in the Mexican axolotl. Dev. Biol 370, 42–51. [PubMed: 22841627]

Zhu SJ, Hallows SE, Currie KW, Xu C, and Pearson BJ (2015). A mex3 homolog is required for differentiation during planarian stem cell lineage development. eLife 4, e07025.

Highlights

- Transposons reactivate during cell differentiation in a lineage-specific manner

- Nuclear SMEDWI-2 preserves chromatin repression at transposons during differentiation

- Chromatin chaperoning by SMEDWI-2 is crucial to facilitate cell fate changes

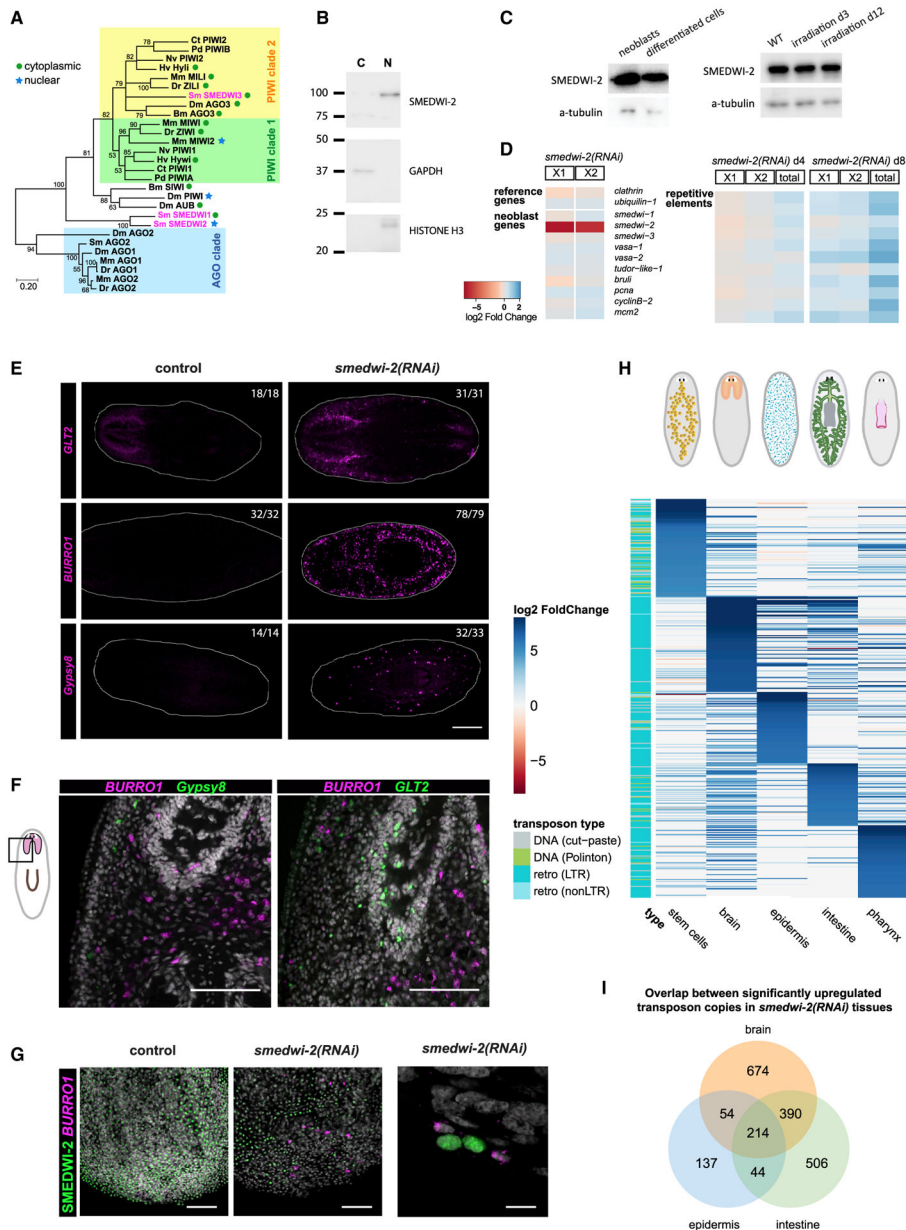- Planarians have two layers of PIWI-based transposon repression in their stem cells

Figure 1. Loss of nuclear PIWI protein SMEDWI-2 leads to tissue-specific desilencing of transposons

(A) Maximum likelihood tree of Argonaute family proteins. Bootstrap values are shown at tree branches.

(B) Western blot of nuclear and cytoplasmic fractions, showing SMEDWI-2 protein in the nucleus.

(C) Western blot of FACS-isolated neoblasts and differentiated cells (left) and of animals in which new cell production has been eliminated for 3 or 12 days (right), showing persistent presence of SMEDWI-2 protein in differentiated cells.

(D) Heatmap showing log2 fold changes of neoblast genes (left) or transposons (right) in G2/M phase neoblasts (X1 cells), G0/G1 phase neoblasts (X2 cells), or total cells at different

time points of *smedwi-2(RNAi)*. The expression levels remain largely unchanged in the neoblasts.

(E) FISH staining of transposon transcripts *BURRO1*, *GLT2*, and *Gypsy8* showing different anatomical patterns. Scale bar, 200 μm.

(F) Double FISH of transposons *BURRO1* (magenta) and *GLT2* or *Gypsy8* (green), showing little overlap in individual cells. Scale bars, 100 μm.

(G) Immunofluorescence for SMEDWI-2 protein (green) with FISH against *BURRO1* (magenta) in *smedwi-2(RNAi)* animals, showing loss of SMEDWI-2 and upregulation of transposon expression in many *smedwi-2(RNAi)* epidermal cells. Scale bars, 100 μm. Right: enlarged. Scale bar, 10 μm.

(H) Schematics of isolated tissues and heatmap showing log2 fold changes in RNA expression of top 100 altered transposons in each *smedwi-2(RNAi)* tissue compared with controls.

(I) Venn diagram of transposon copies with significantly upregulated RNA expression in *smedwi-2(RNAi)* brain, epidermis, and/or intestine.

Bm, Bombyx mori; Ct, Capitella teleta; Dm, *Drosophila melanogaster*; Dr, Danio rerio; Hv, Hydra vulgaris; Mm, *Mus musculus*; Nv, Nematostella vectensis; Pd, Platynereis dumerilii; Sm, Schmidtea mediterranea.
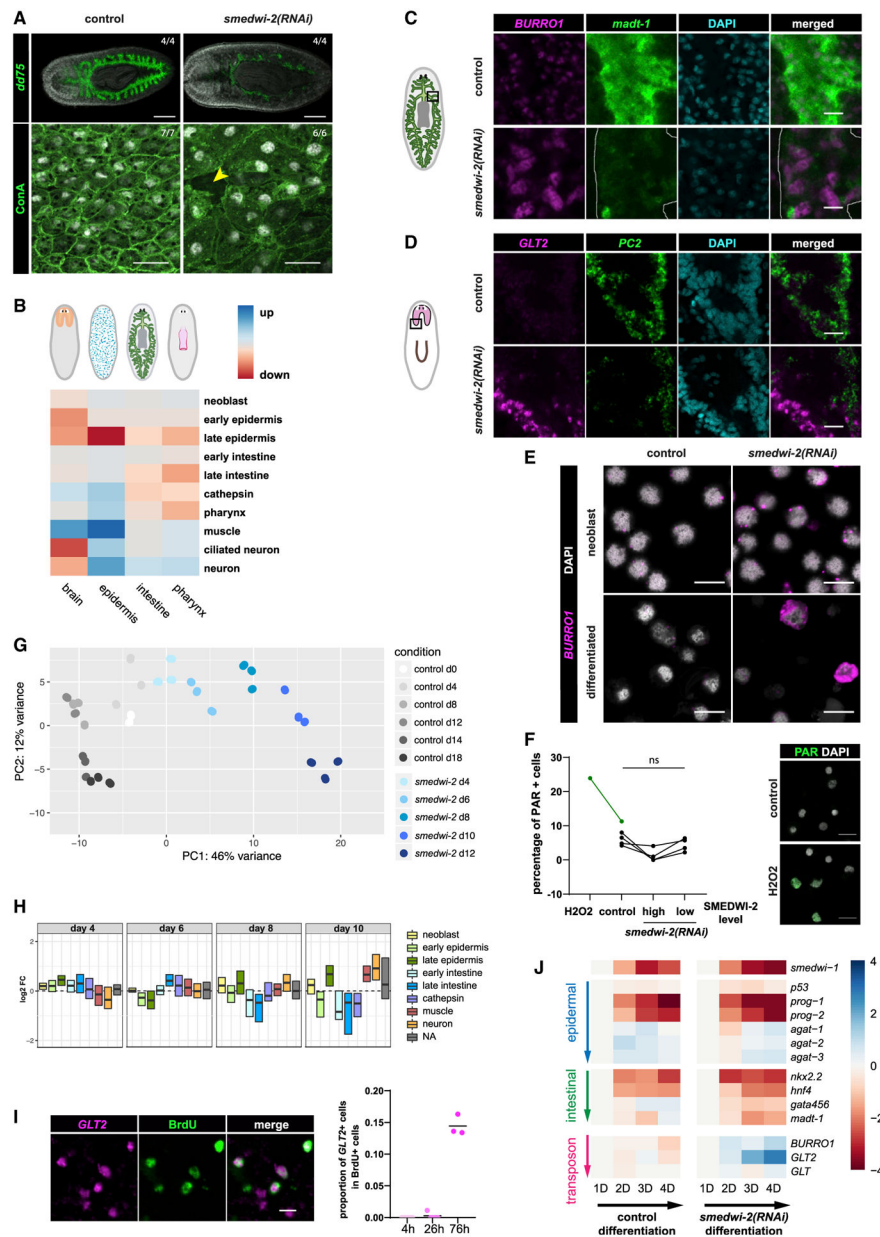
Figure 2. Tissue-specific gene expression is progressively deregulated in *smedwi-2(RNAi)*

(A) Top: FISH of intestinal marker *dd75* shows degenerated intestine in day (d) 10 *smedwi-2(RNAi)* animals. Scale bars, 200 μm. Bottom: concanavalin A (Con A) staining shows disorganized ventral epidermis with reduced cell density, deformed nuclei, and small lesions (yellow arrowhead) in *smedwi-2(RNAi)* animals at endpoint. Scale bars, 20 μm.

(B) Schematic of the isolated tissues and heatmap showing the summarized expression changes upon *smedwi-2(RNAi)* of genes expressed in each of the indicated tissue types.

(C and D) Double FISH of *BURRO1* (magenta) with intestinal marker *madt-1* (green) (C) or *GLT2* (magenta) with neuronal marker *PC2* (green) (D) in control and *smedwi-2(RNAi)* animals. Transposon-expressing cells are found in the differentiated tissues but fail to express the appropriate tissue markers. Scale bars, 20 μm.

(E) FISH of *BURRO1* (magenta) in FACS-isolated neoblasts (X1) or differentiated cells (Xins) from control or *smedwi-2(RNAi)* animals showing transposon upregulation in live, differentiated cells. Scale bars, 10 μm.

(F) Immunostaining of poly-ADP ribose (PAR) in control, *smedwi-2(RNAi)*, and 1 mM H_2O_2-treated differentiated cells (Xins). Left: quantification of four separate experiments showing no increase of DNA damage in *smedwi-2(RNAi)* cells. Right: representative images. Scale bars, 10 μm.

(G) Principal-component analysis (PCA) of time-course RNA-seq data from *smedwi-2(RNAi)* total cells. PC1 increasingly separates *smedwi-2(RNAi)* samples from controls starting at d4.

(H) Log2 fold change of lineage-specific genes showing progressive loss of expression of epidermal and intestinal lineage markers in *smedwi-2(RNAi)* animals.

(I) Right: proportion of BrdU$^+$ cells expressing *GLT2* after different chase periods. Transposon upregulation is observed 3 days after cell-cycle exit. Left: representative image showing BrdU$^+$ cells with *GLT2* expression (white arrowheads). Scale bar, 10 μm.

(J) Log2 fold change of lineage markers in EdU-labeled control and *smedwi-2(RNAi)* differentiating cells. EdU$^+$ cells were isolated by FACS at corresponding days after EdU feed. Gene expression was measured by qPCR and normalized to the d1 cells.
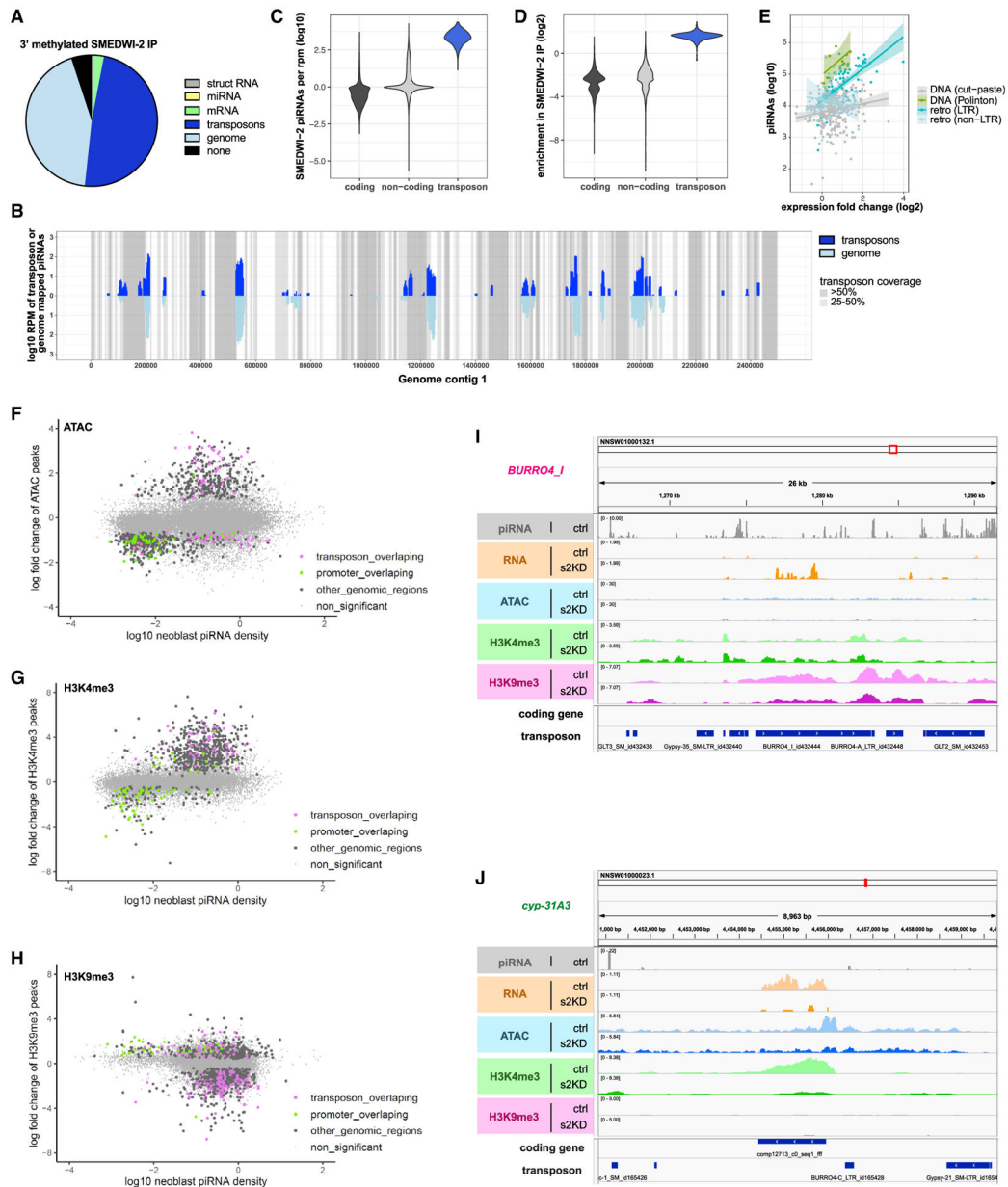
Figure 3. SMEDWI-2 targets transposon-rich regions on the chromatin level

(A) Mapping composition of β-eliminated SMEDWI-2-bound small RNA.

(B) Log10 reads per million (RPM) of uniquely perfectly mapped SMEDWI-2-bound piRNAs over a 2.5-Mb region of the genome. Note that many transposon regions are repetitive and contain few uniquely mapped reads.

(C) piRNA abundance normalized to transcript abundance. Only transposons have high numbers of piRNAs relative to transcript abundance.

(D) piRNA enrichment in SMEDWI-2 IP versus input. Only transposon mapping piRNAs are enriched in SMEDWI-2 IP.

(E) Correlation of transposon piRNA abundance and expression changes upon *smedwi-2(RNAi)*. LTR retrotransposons and Polintons show a clear correlation between

piRNA abundance and expression upregulation, suggesting that they are directly repressed by SMEDWI-2.

(F–H) Log2 fold change in *smedwi-2(RNAi)* of ATAC (F), H3K4me3 (G), or H3K9me3 (H) peaks in relation to piRNA density. Significantly changed peaks overlapping transposons or gene promoters are shown in magenta and green, respectively. Transposon overlapping peaks tend to show increased accessibility, increased H3K4me3, and/or decreased H3K9me3 signal upon *smedwi-2(RNAi)*, while some gene promoter peaks not targeted by piRNAs show decreased accessibility, decreased H3K4me3, or increased H3K9me3 modifications.

(I and J) Genome browser view showing piRNA targeted transposon copy *BURRO4* upregulated upon *smedwi-2(RNAi)* (I) and non-targeted coding gene *cyp-31A3* downregulated upon *smedwi-2(RNAi)* (J).

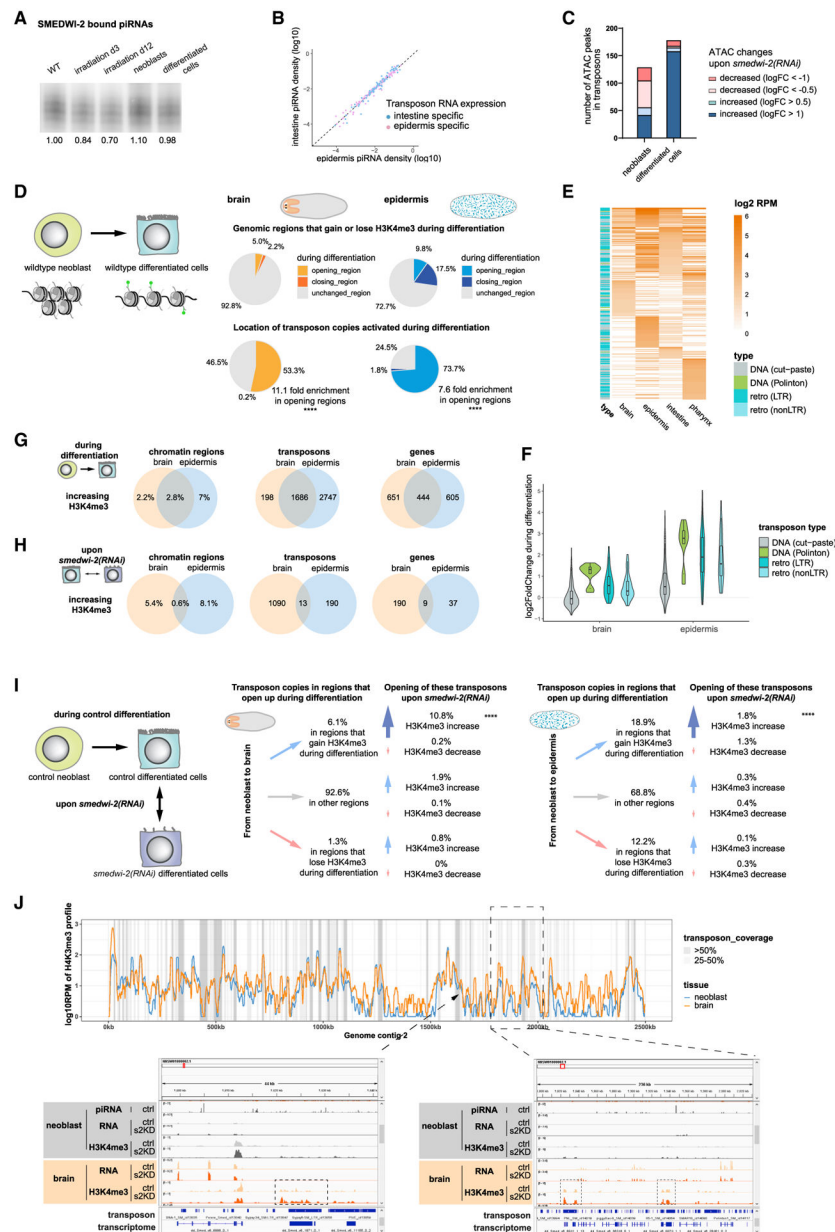Ctrl, control; s2KD, *smedwi-2(RNAi)*.

Figure 4. Changes in chromatin accessibility during differentiation sensitize regions in a tissue-specific manner

(A) Autoradiogram of piRNAs precipitated with the same amount of SMEDWI-2 from different cell populations, showing that SMEDWI-2 protein is loaded with piRNAs in differentiated cells. Normalized quantification of signal is shown under each lane.

(B) Correlation of epidermal and intestinal piRNA density on transposon copies with tissue-specific RNA upregulation in *smedwi-2(RNAi)*.

(C) Changes in transposon-overlapping ATAC peaks in *smedwi-2(RNAi)* neoblasts and differentiated cells showing stronger deregulation in differentiated cells.

(D) Chromatin changes during wild-type differentiation from neoblast to brain or epidermis. Left: schematic. Top right: fraction of the genome that gains (light) or loses (dark)

H3K4me3 during differentiation. Bottom right: fraction of activating transposon copies located in each of these genomic regions.

(E) Heatmap of log2 RPM of top 100 abundant transposons in the indicated tissues of control animals. Baseline expression of transposons is already tissue specific.

(F) Violin plots showing H3K4me3 increase in different classes of transposons during differentiation from control neoblasts to neuronal or epidermal lineage. LTR retroelements and Polintons are desilenced during normal differentiation.

(G) Venn diagrams of activated genomic regions during wild-type cell differentiation. Activated regions are tissue specific. Changes are stronger in epidermis than in brain.

(H) Venn diagrams representing activation of genomic regions because of loss of SMEDWI-2. Activated regions and transposon copies are strongly tissue specific.

(I) Horizontal arrows indicate the percentage of transposon copies located in significantly opening, closing, or unchanged chromatin regions during the differentiation from control neoblasts to brain or epidermis. Vertical arrows represent the percentage of transposon copies within each category that show significant chromatin state changes upon *smedwi-2(RNAi)*. Transposons that decondense upon *smedwi-2(RNAi)* are significantly enriched in chromatin regions that already open during normal differentiation (**** p < 0.0001).

(J) Top: H3K4me3 profile of control neoblasts (blue) and brain (orange) over a 2.5-Mb genome region. Bottom: genome browser views of loci with opening chromatin and increasing gene expression during normal differentiation and further opening of transposon copies (dashed boxes) upon *smedwi-2(RNAi)*.
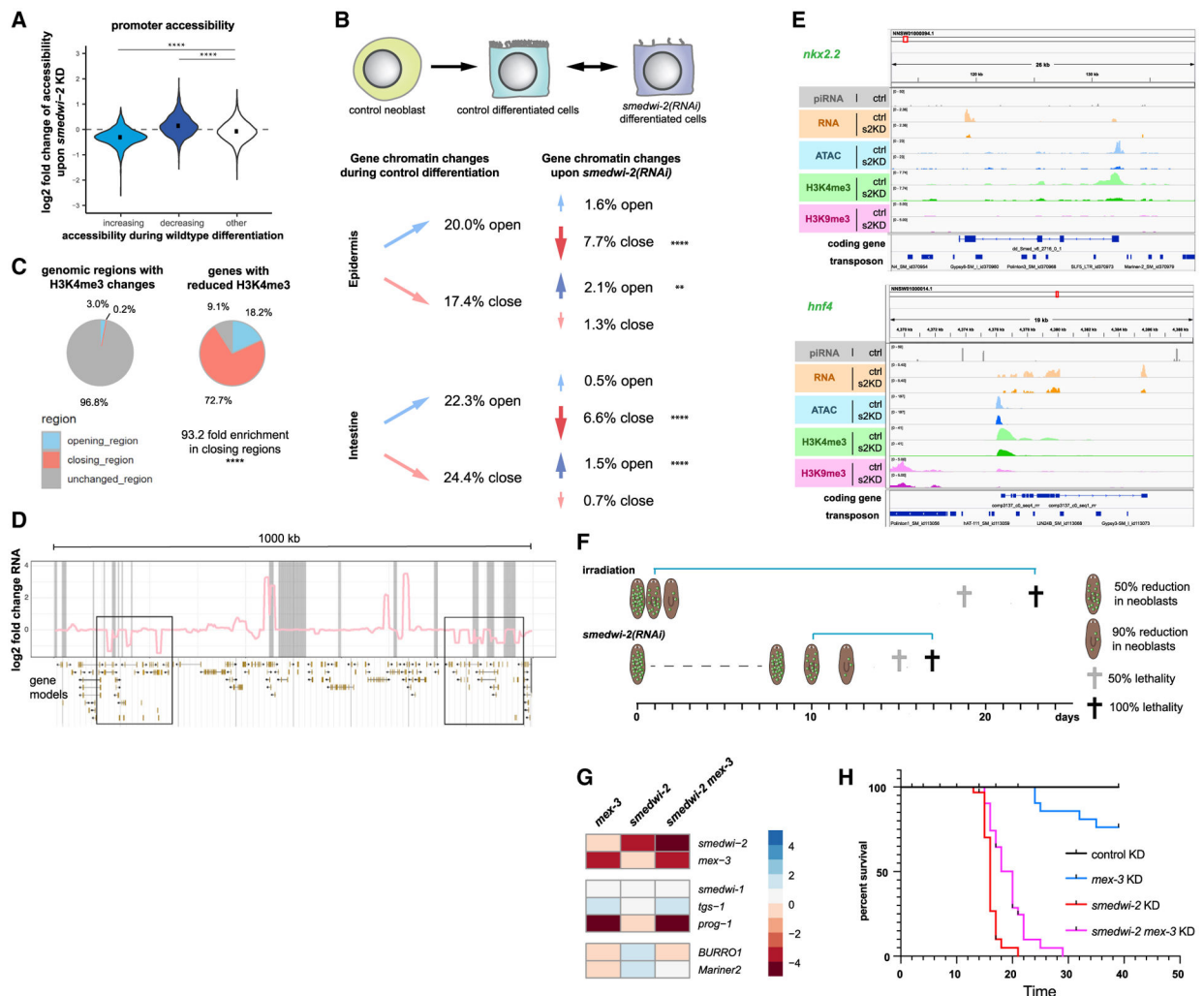
Figure 5. SMEDWI-2 knockdown leads to deregulated cells that have a detrimental effect on animal health

(A) Violin plots showing genes with altered promoter accessibility during normal differentiation from neoblasts to epidermis and their changes upon *smedwi-2(RNAi)*. ****p < 0.0001, by Mann-Whitney U test. Genes with increased accessibility during normal differentiation tend to be less upregulated upon *smedwi-2(RNAi)* and vice versa.

(B) Horizontal arrows indicate the percentage of genes upregulated or downregulated during the differentiation from control neoblasts to epidermis or intestine. Vertical arrows represent the percentage of genes within each category that show significant changes upon *smedwi-2(RNAi)*. Asterisks indicate the significance of enrichment. Genes that are downregulated upon *smedwi-2(RNAi)* are significantly enriched among genes that are normally upregulated during differentiation.

(C) Although only minor regions of the genome gain (blue) or lose (red) H3K4me3 (left) in *smedwi-2(RNAi)*; genes that decrease (right) in H3K4me3 are clustered in those regions.

(D) 1-Mb genome window showing several domains of clustered genes with reduced expression upon *smedwi-2(RNAi)*.

(E) Genome browser view showing downregulation of intestinal transcription factors *nkx2.2* and *hnf-4* in *smedwi-2(RNAi)* neoblasts.

(F) Schematic of the timeline of animal survival and neoblast loss in *smedwi-2(RNAi)* compared with γ-irradiated animals. Blue brackets: time span between neoblast loss and animal lethality.

(G and H) Inhibition of cell differentiation by *mex-3* knockdown results in partial rescue of the *smedwi-2(RNAi)* phenotype. (G) Log2 fold change of gene expression in *mex-3(RNAi)*, *smedwi-2(RNAi)*, and *mex-3 smedwi-2(double RNAi)* animals relative to control, measured by qPCR. *Mex-3(RNAi)* shows a decrease in cell differentiation marker *prog-1* and an increase in neoblast marker *tgs-1*. (H) Survival curve of *mex-3(RNAi)*, *smedwi-2(RNAi)*, and *mex-3 smedwi-2(dRNAi)* animals. *Mex-3 smedwi-2(dRNAi)* animals show delayed transposon upregulation and significantly longer lifespan than *smedwi-2(RNAi)* animals (p < 0.0001 by log rank test; n = 20; 3 replicates).
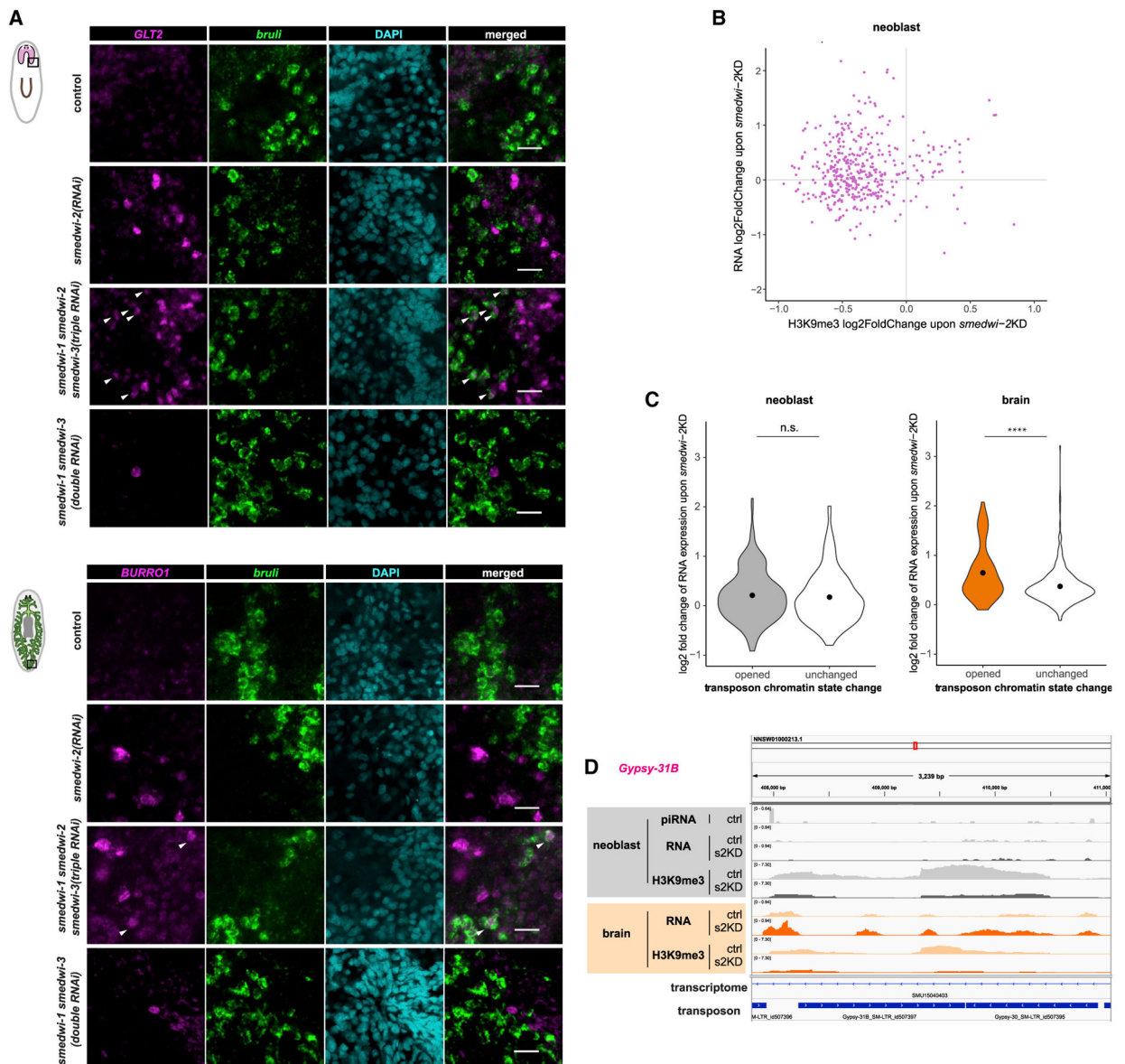
Figure 6. Neoblasts have a double layer of protection against transposon activation

(A) Double FISH against *GLT2* or *BURRO1* (magenta) and neoblast marker *bruli* (green) in control, *smedwi-2(RNAi)*, *smedwi-1/2/3(triple RNAi)*, and *smedwi-1/3(double RNAi)* animals. Arrowheads indicate transposon-expressing neoblasts in the triple RNAi animals. Scale bars, 20 μm.

(B) Scatter plot showing H3K9me3 and RNA changes of transposons in *smedwi-2(RNAi)* neoblasts. Many transposons with decreased H3K9me3 modification remain unchanged at the RNA level.

(C) Violin plots showing log2 RNA fold change of transposons with opened or unchanged chromatin states in *smedwi-2(RNAi)* neoblasts and brain. Opened transposons show RNA upregulation in *smedwi-2(RNAi)* brain, but not in neoblasts.**** p<0.0001, by Mann-Whitney U test.

(D) Genome browser view of a transposon copy *Gypsy-31B* with decreased H3K9me3 modification and unchanged RNA expression in *smedwi-2(RNAi)* neoblasts but upregulated expression in *smedwi-2(RNAi)* brain.
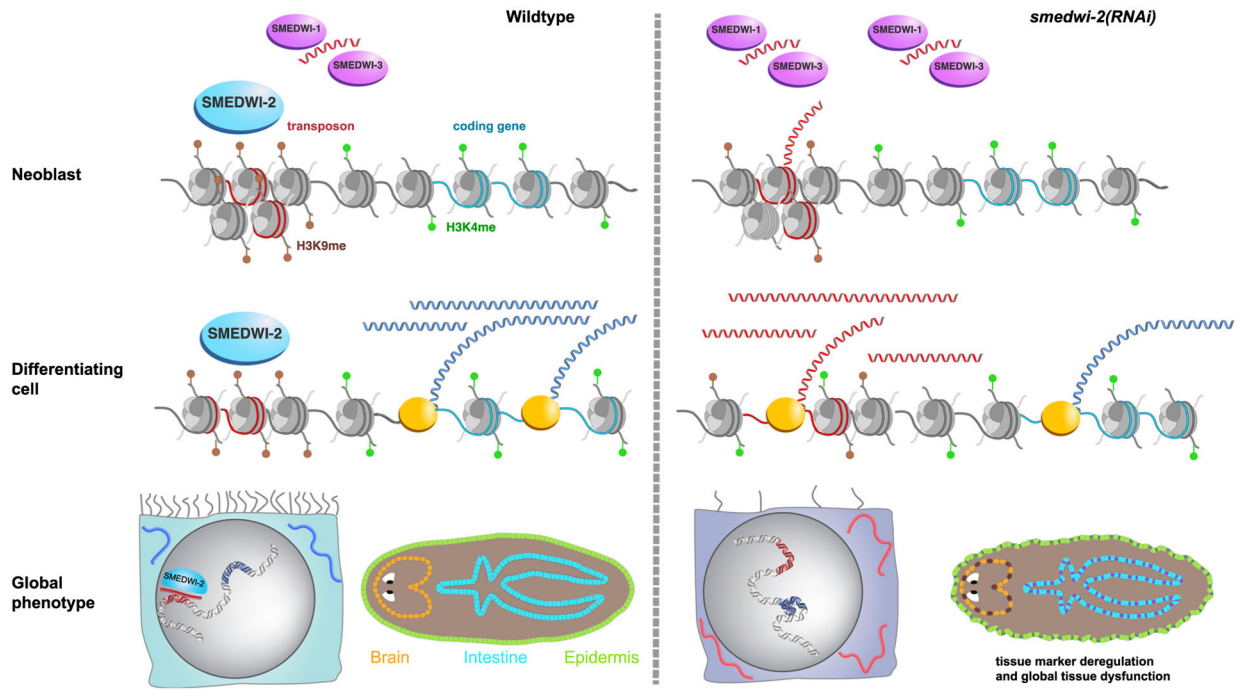
Figure 7. Model of SMEDWI-2 function in planarian stem cell biology
See main text.

KEY RESOURCES TABLE

REAGENT or RESOURCE	SOURCE	IDENTIFIER
Antibodies		
Rabbit polyclonal anti-SMEDWI-2 protein antibody	This paper	N/A
Rabbit polyclonal anti-SMEDWI-2 peptide antibody	This paper	N/A
Rabbit anti-phospho-Histone H3 (Ser10) Antibody, clone 63-1C-8	Millipore	Cat# 05–817R; RRID:AB_11215621
Mouse anti-BrdU antibody, clone B44	BD Biosciences	Cat# 347580; RRID:AB_400326
Mouse anti-poly-ADP-ribose antibody, clone 10H	Santa Cruz Biotechnology	Cat# sc-56198; RRID: AB_785249
Rabbit anti-GAPDH antibody	Proteintech	Cat# 10494–1-AP; RRID:AB_2263076
Rabbit anti-Histone H3 antibody	Abcam	Cat# ab1791; RRID:AB_302613
Rabbit anti-H3K4me3 antibody	Millipore	Cat# 07–473; RRID:AB_1977252
Rabbit anti-H3K9me3 antibody	Abcam	Cat# ab8898; RRID:AB_306848
Mouse anti-α-tubulin antibody	Millipore	Cat# MABT205; RRID:AB_11213030
anti-digoxigenin-POD, Fab fragments	Roche	Cat# 11 207 733 910; RRID: AB_514500
anti-fluorescein-POD, Fab fragments	Roche	Cat# 11 426 346 910; RRID: AB_840257
anti-DNP-HRP conjugate	Perkin-Elmer	Cat# FP1129; RRID: AB_2629439
Goat anti-rabbit HRP conjugate	Thermo Fisher Scientific	Cat# G-21234; RRID:AB_2536530
Goat anti-mouse HRP conjugate	Thermo Fisher Scientific	Cat# G-21040; RRID:AB_2536527
Goat anti-rabbit AF568 conjugate	Thermo Fisher Scientific	Cat# A-11036; RRID:AB_10563566
Goat anti-mouse AF488 conjugate	Thermo Fisher Scientific	Cat# A-11029; RRID:AB_138404
Chemicals, peptides, and recombinant proteins		
SMEDWI-2 peptide for antibody generation KKPMRRERKKKDEEGVE	This paper	N/A
pA-Tn5 Transposase	Diagenode	Cat# C01070002–30
Critical commercial assays		
Alexa Fluor Tyramide SuperBoost Kit	Invitrogen	Cat# B40943
TruSeq RNA Library Prep Kit v2	Illumina	Cat# RS-122–2001
Deposited data		
Raw sequencing data	This paper	SRA: PRJNA633618
Schmidtea mediterranea S2F2 genome SMESG.1	(Grohme et al., 2018)	http://planmine.mpi-cbg.de/planmine/begin.do
Schmidtea mediterranea dd_v6 transcriptome	(Liu et al., 2013)	http://planmine.mpi-cbg.de/planmine/begin.do
Schmidtea mediterranea unigene transcriptome	(Robb et al., 2015)	http://planmine.mpi-cbg.de/planmine/begin.do
Schmidtea mediterranea transposon consensus	(Bao et al., 2015)	https://www.girinst.org/repbase/
Experimental models: Organisms/strains		
Schmidtea mediterranea, clonal strain CIW4, asexual	Laboratory of Josien van Wolfswinkel	N/A
Oligonucleotides		
Sequences used for all FISH probes and dsRNA, as well as primers used for cloning and qRT-PCR are provided in Table S1	N/A	N/A
3' adaptor for small RNA library generation: rAppTGGAATTCTCGGGTGCCAAGG/ddC/	(Shore et al., 2016)	N/A

REAGENT or RESOURCE	SOURCE	IDENTIFIER
5' adaptor for small RNA library generation: GUUCAGAGUUCUACAGUCCGACGAUC	(Shore et al., 2016)	N/A
RT primer for small RNA library generation: GCCTTGGCACCCGAGAATTCCA	(Shore et al., 2016)	N/A
Recombinant DNA		
pET28-SMEDWI-2(1–166)-PP-GST	This paper	N/A
pTXB1-Tn5	(Picelli et al., 2014)	RRID:Addgene_60240
Software and algorithms		
ZEN Digital Imaging for Light Microscopy	Zeiss	RRID:SCR_013672; https://www.zeiss.com/microscopy/us/products/microscope-software/zen.html
ImageJ (FIJI)	(Schindelin et al., 2012)	RRID:SCR_002285; https://fiji.sc
GraphPad Prism	GraphPad Software	RRID:SCR_002798; https://www.graphpad.com/scientific-software/prism/
R Project for Statistical Computing	The R Foundation	RRID: SCR_001905; https://www.r-project.org/
FastQC	(Andrews, 2010)	RRID:SCR_014583; https://www.bioinformatics.babraham.ac.uk/projects/fastqc/
Cutadapt	(Martin, 2011)	RRID:SCR_011841; https://cutadapt.readthedocs.io/en/stable/
Bowtie	(Langmead, 2010)	RRID:SCR_005476; http://bowtie-bio.sourceforge.net/index.shtml
Bowtie2	(Langmead and Salzberg, 2012)	http://bowtie-bio.sourceforge.net/bowtie2/manual.shtml
Samtools	(Li et al., 2009b)	RRID:SCR_002105; http://samtools.sourceforge.net
STAR	(Dobin et al., 2013)	RRID:SCR_015899; https://github.com/alexdobin/STAR
RepeatMasker	(Smit et al., 2013)	RRID:SCR_012954; http://repeatmasker.org/
Telescope	(Bendsall et al., 2019)	https://github.com/mlbendall/telescope
DESeq2	(Love et al., 2014)l	RRID:SCR_015687; https://bioconductor.org/packages/release/bioc/html/DESeq2.html
Picard	Broad Institute	RRID:SCR_006525; http://broadinstitute.github.io/picard/
Genrich	Gaspar, 2018	https://github.com/jsh58/Genrich
MACS2	(Gaspar, 2018)	RRID:SCR_013291; http://liulab.dfci.harvard.edu/MACS/
BEDTool	(Quinlan, 2014)	RRID:SCR_006646; https://github.com/arq5x/bedtools2
DiffBind	(Stark and Brown, 2011; Ross-Innes et al., 2012)	RRID:SCR_012918; http://bioconductor.org/packages/release/bioc/html/DiffBind.html
ggplot2	(Wickham 2016)	RRID:SCR_014601; https://cran.r-project.org/web/packages/ggplot2/index.html
IGV	(Robinson et al., 2017)	RRID:SCR_011793; https://www.broadinstitute.org/igv/